Science of the Total Environment 793 (2021) 148635

Contents lists available at ScienceDirect

Science of the Total Environment

journal homepage: www.elsevier.com/locate/scitotenv

Changes in groundwater trace element concentrations before seismic and volcanic activities in Iceland during 2010–2018

Maurizio Barbieri [a,*], Stefania Franchini [a], Marino Domenico Barberio [a], Andrea Billi [b], Tiziano Boschetti [c], Livio Giansante [a], Francesca Gori [a], Sigurjón Jónsson [d], Marco Petitta [a], Alasdair Skelton [e], Gabrielle Stockmann [f]

[a] Earth Sciences Department, Sapienza University of Rome, Rome, Italy
[b] Consiglio Nazionale delle Ricerche, IGAG, Rome, Italy
[c] Department of Chemistry, Life Sciences and Environmental Sustainability, University of Parma, Italy
[d] King Abdullah University of Science and Technology (KAUST), Saudi Arabia
[e] Department of Geological Sciences, Stockholm University, Stockholm, Sweden
[f] Institute of Earth Sciences, University of Iceland, Reykjavík, Iceland

HIGHLIGHTS

- Boron appears to be a good indicator of water-rock interaction in a geothermal system.
- PCA was used to identify the specific role of elements in different geologic events.
- CPD used to statistically validate of the trend variability in the time series
- Trace elements are promising to identify potential precursors of geological events.

GRAPHICAL ABSTRACT

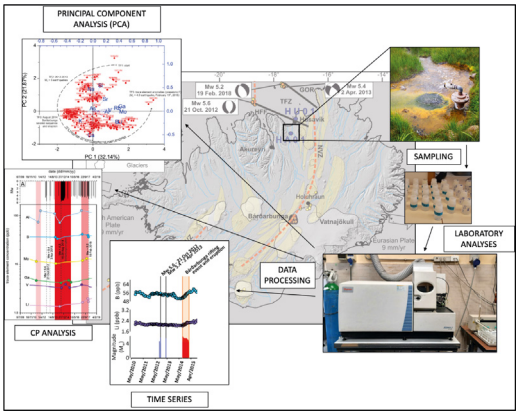

ARTICLE INFO

Article history:
Received 27 April 2021
Received in revised form 8 June 2021
Accepted 19 June 2021
Available online 24 June 2021

Editor: Jurgen Mahlknecht

Keywords:
Seismic precursors
Volcanic precursors
Hydrogeochemical anomalies
Earthquakes
Pre-seismic processes
Bárðarbunga

ABSTRACT

We analysed temporal variations of trace element concentrations in groundwater from a 101 m-deep borehole (HA01) in northern Iceland during 2010–2018 and compared them with seismic and volcanic events that occurred in the same period to identify potential hydrogeochemical precursors. An increase of B, Al, V, Li and Mo concentrations started from eight months to one month before the 2014 Bárðarbunga eruption (~115 km from HA01), a major rifting event in central Iceland, while Ga and V concentrations began to increase one day and one month after the onset of the event, respectively. We also found that concentrations of some trace elements (Li, B, Ga, Mo, Sr, Rb and Fe) significantly increased before an M_w 5.0 earthquake that occurred ~80 km from the borehole in 2018. However, other notable hydrogeochemical changes were detected during the monitoring period without apparent correlation with the seismic and volcanic events in the region. This study shows that the systematic long-term hydrogeochemical monitoring in seismic and volcanic areas is critical to advance the science of seismic and eruptive precursors. Furthermore, the use of statistical tools, such as Principal Component Analysis (PCA) and Change Point (CP) detection can help identify the most useful chemical elements and validate the trend variability of those elements in the time series, reducing arbitrary choices of pre-seismic and pre-volcanic hydrogeochemical anomalies as potential precursors.

* Corresponding author.
E-mail address: maurizio.barbieri@uniroma1.it (M. Barbieri).

https://doi.org/10.1016/j.scitotenv.2021.148635
0048-9697/

1. Introduction

Hydrogeochemical changes related to earthquakes have been documented throughout history (Manga and Wang, 2015; Wang and Manga, 2021). Most of these changes were recorded in conjunction with and/or after seismic events (Scholz et al., 1973; Wakita, 1975; Igarashi et al., 1995; Montgomery and Manga, 2003; Manga et al., 2003; Cucci, 2019; Kim et al., 2019; Barberio et al., 2020; Chiodini et al., 2020; Barbieri et al., 2020; Hosono and Masaki, 2020; Kawabata et al., 2020; Sato et al., 2020); however, recent anomalous hydrogeochemical variations before $M_w \geq \sim 5$ earthquakes have been systematically measured and documented (Claesson et al., 2004; Chen et al., 2013; Skelton et al., 2014, 2019; Chen et al., 2015; Barberio et al., 2017; Petitta et al., 2018; De Luca et al., 2018; Onda et al., 2018; Boschetti et al., 2019; Sano et al., 2020). Until recently, the lack or paucity of continuous and long-term hydrogeochemical monitoring aimed at investigating the seismic cycle (Ingebritsen and Manga, 2014; Skelton et al., 2019; Zhou et al., 2020) have significantly limited the ability of scientists to identify and fully understand any seismic precursors of a hydrogeochemical nature. While seismological and geodetic (GPS) networks have been globally active for many years and have provided important information about crustal deformation and seismic cycles (e.g., Chiarabba et al., 2020), hydrogeochemical networks for seismic precursor identification have only recently started to emerge in China, Iceland, Italy, Japan, western USA and a few other countries (Chaudhuri et al., 2013; Hosono and Masaki, 2020; Franchini et al., 2020). These new networks, or single monitoring stations, have produced significant results on pre-seismic hydrogeochemical changes likely connected with the dilatative preparatory phases of intermediately strong earthquakes. In particular, pre-earthquake changes in groundwater temperature (Shi and Wang, 2014; He and Singh, 2019), chemical composition (Claesson et al., 2004; Barberio et al., 2017; Onda et al., 2018; Boschetti et al., 2019; Skelton et al., 2019; Hosono et al., 2020; Nakagawa et al., 2020; Shi et al., 2020; Franchini et al., 2020) and changes in natural gas geochemistry (Wakita et al., 1980; King et al., 2006; Sano et al., 2016; Barbieri, 2019; Buttitta et al., 2020; Martinelli et al., 2020) have been properly documented and interpreted as potential seismic precursors. Fossil instances of seismic precursors are also starting to be documented in fault-related mineralization (Andrén et al., 2016; Coppola et al., 2021) near where hydrogeochemical precursors of strong earthquakes had previously documented in northern Iceland and central Italy (Skelton et al., 2014; Barberio et al., 2017).

Hydrogeochemical monitoring networks are now emerging for seismic precursor identification, whereas volcanic eruption precursors are mainly searched for and identified through seismic and geodetic monitoring (Patanè et al., 2003; Sparks, 2003; McNutt and Roman, 2015) or through geochemical measurements often (but not only) on proximal emissions, such as fumaroles, hot springs and volcanic lakes (Aiuppa et al., 2007; De Moor et al., 2016). Conversely, the intermediate or remote hydrogeochemical monitoring of volcanoes for eruption precursor identification, although used, is rarer (Armienta and De la Cruz-Reyna, 1995; Caracausi et al., 2003). Below, we will show that this remote method could be more suitable, more reliable, and easier than sampling proximal volcanic fluid emissions.

Since 2002, a hydrogeochemical monitoring system has been running in northern Iceland with the main aim of identifying potential precursors to earthquakes. One monitoring station was set up at Húsavík (HU01) and the other at Hafralækur (HA01) (Claesson et al., 2004, 2007; Skelton et al., 2014, 2019; Andrén et al., 2016). The samples from this study come from HA01 that consists of a 101 m-deep borehole located at Lat. 65.8722°N and Long. 17.4528°W (Fig. 1). HA01 has been continuously monitored since 2008. The monitoring system has allowed geoscientists to identify hydrogeochemical changes (interpreted as potential seismic precursors) before three large earthquakes ($M_w > 5.0$) that occurred off northern Iceland on 16 September 2002, 21 October 2012 and 2 April 2013. Before the 2012 M_w 5.6 and the 2013 M_w 5.4 earthquakes, significant anomalies in groundwater concentrations of Na, Ca, Si, $\delta^{18}O$ and $\delta^{2}H$ were recorded at the HA01 hydrogeochemical station (Skelton et al., 2014). These studies were then followed by geochemical modelling and statistical studies to explain and verify previous interpretations (Andrén et al., 2016; Skelton et al., 2019). Moreover, before the 2002 M_w 5.8 earthquake, significant anomalies of Cu, Zn, Mn and Cr were detected in groundwater from the HU01 borehole (20 km from the HA01 borehole) at Húsavík (Skjálfandi Bay; Fig. 1) together with pre- and post-seismic shifts of groundwater concentrations of B, Ca, K, Li, Mo, Na, Rb, S, Si, Sr, Cl, SO_4, $\delta^{18}O$ and $\delta^{2}H$ (Claesson et al., 2004).

In 2018, to expand the hydrogeochemical analyses of the monitored HA01 groundwater and identify further potential precursors of earthquakes in northern Iceland, international collaboration was established between Stockholm University, the University of Iceland at Reykjavík, Sapienza University of Rome and CNR-IGAG in Rome. Within this collaboration, we analysed trace element concentrations in the groundwater sampled from the HA01 borehole between 2010 and 2018 together with earthquake and volcanic data in the same period.

We then used geochemical-thermodynamic computations to constrain the origin of the observed elements. The results show new potential hydrogeochemical precursors of $M_w \geq \sim 5$ earthquakes and remote hydrogeochemical precursors of volcanic eruptions. These results are integrated with previous hydrogeochemical findings obtained from the same monitoring system (Skelton et al., 2019) for a better comprehension of the hydrogeochemical and physical processes that occur during the preparatory phases of intermediately strong earthquakes and volcanic eruptions in Iceland.

Our main aim is to advance the science of hydrogeochemical precursors of earthquakes and volcanic eruptions. Our results are part of a tentative first step towards forming the background necessary to formulate national protocols aimed at seismic and volcanic precursor identification and related hazard mitigation.

2. Geological and hydrogeological settings

Iceland is located on the Mid-Atlantic Ridge between the divergent plate margins of Eurasia to the east, North America to the west, the Reykjanes ridge to the south and the Kolbeinsey ridge to the north (Einarsson, 1991; Einarsson et al., 2008; Árnadottir et al., 2008; Fig. 1). The tectonic setting of Iceland is dominated by an eastward shift of the Mid-Atlantic Ridge due to a hot spot currently located under the Vatnajökull glacier in southeastern Iceland (Thordarson and Larsen, 2007). Two transform zones connect the shifted ridge segment to the Mid-Atlantic Ridge: the South Iceland Seismic Zone (SISZ) to the south and the Tjörnes Fracture Zone (TFZ) to the north (Fig. 1). The TFZ cuts across the area investigated in this work in northern Iceland.

The TFZ is a 120 km-long and 70 km-wide oceanic oblique transform zone linking the Northern Volcanic Rift Zone to the south and the southern end of the submarine Kolbeinsey ridge to the north (Einarsson, 1991; Einarsson et al., 2008; Stefansson et al., 2008). This WNW-ESE-trending fracture zone includes two main transform structures: the Grímsey Oblique Rift (GOR) and the Húsavík-Flatey Fault (HFF) (Gudmundsson et al., 1993; Gudmundsson, 2007; Rögnvaldsson et al., 1998; Stefansson et al., 2008; Wästeby et al., 2014; Tibaldi et al., 2020; Fig. 1).

Seismic activity in Iceland is mainly linked to the extensional and lateral transfer dynamics associated with Mid-Atlantic Ridge kinematics. Therefore, seismic activity is mainly located along the ridge segments, but it is rarer in intraplate areas. Earthquakes in northern Iceland occur mainly in the TFZ (Gudmundsson, 2007) along the HFF and GOR (IMO, 2016; Fig. 1). Strike-slip and normal fault motions in the TFZ are responsible for the high level of seismic activity in this zone, which has hosted more than 10 $M_w > 6$ earthquakes in the past 300 years (Gudmundsson et al., 1993; Gudmundsson, 2007; Rögnvaldsson et al., 1998; Stefansson et al., 2008; Wästeby et al., 2014; Skelton et al., 2019). Additionally, moderately strong earthquakes have been recorded

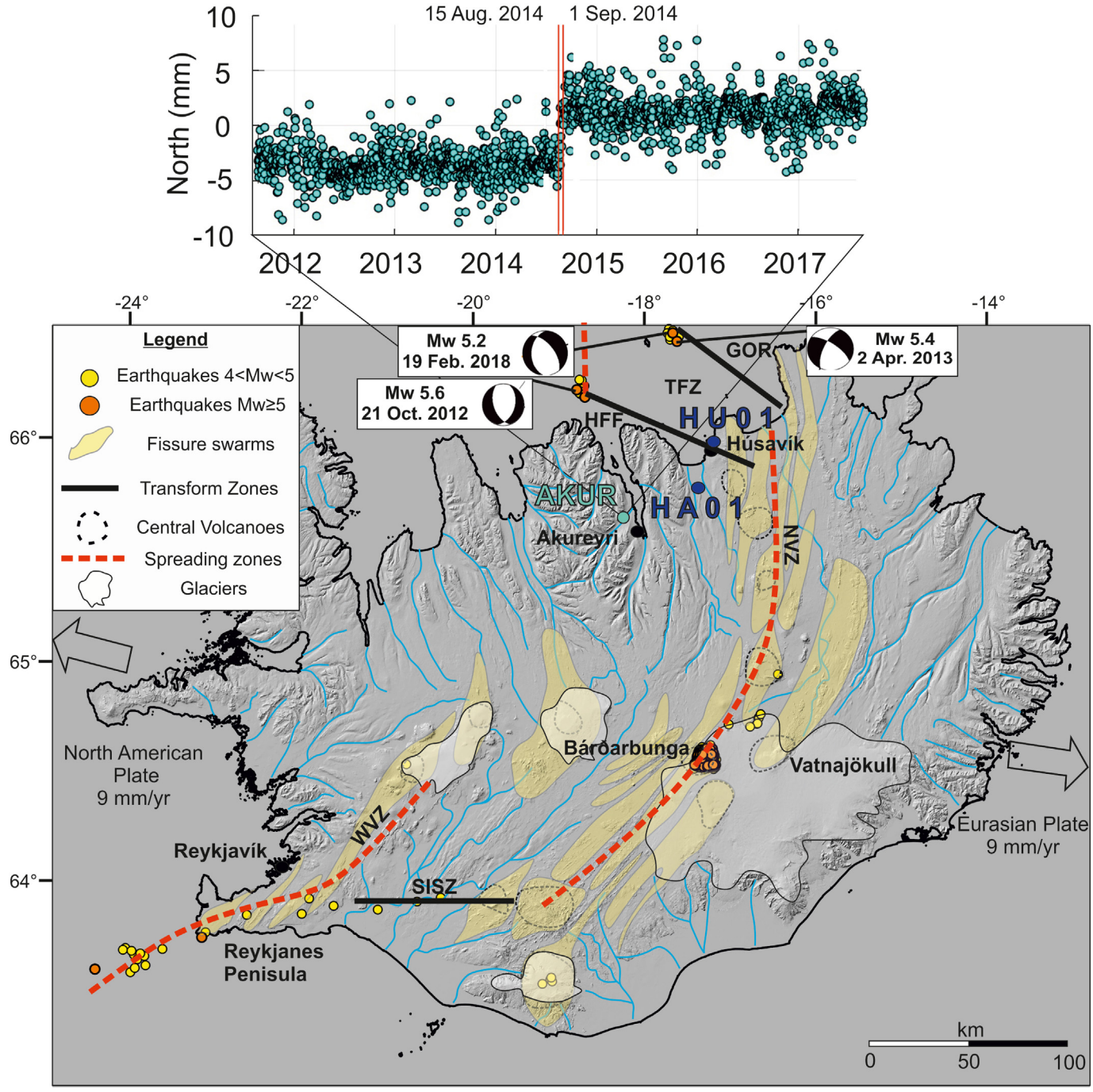

Fig. 1. Map of Iceland. Groundwater sampling sites in Hafralækur (HA01) and Húsavík (HU01), northern Iceland, are displayed with blue symbols. CGPS station (AKUR) in northern Iceland and the relative time series of the detrended north component are displayed with turquoise circles (see the diagram on top of the map; modified after Jónsson et al., 2019). The CGPS time series shows a ~5 mm transient signal due to the Bárðarbunga-Holuhraun dike intrusion. The red vertical lines mark 15 August and 1 September 2014, just before and after the diking activity. In the map, the Bárðarbunga volcano and glaciers (e.g., Vatnajökull) are also shown. Spreading zones and main transform zones are represented with red dotted lines and black solid lines, respectively. Fissure swarms are displayed as yellow shaded areas (from Árnason, 2020). Earthquake epicenters (2010–2018) are represented with orange and yellow dots depending on the magnitude (https://en.vedur.is/). Focal mechanisms of selected earthquakes (October 21st, 2012, Mw 5.6; April 2nd, 2013, Mw 5.4; August 16th, 2014, Mw 4.0; February 19th, 2018, Mw 5.2) are also shown (https://en.vedur.is/). (For interpretation of the references to color in this figure legend, the reader is referred to the web version of this article.)

along with volcanic activity, such as at Katla, Krafla and Bárðarbunga (Einarsson and Björnsson, 1979; Einarsson et al., 2008).

During our monitoring period (2010–2018), the main seismic and volcanic events that occurred in central and northern Iceland were four $M_w \geq 5.0$ earthquakes in the TFZ and one volcanic eruption (a rifting event). The earthquakes occurred off northern Iceland along the western HFF on 21 October 2012 (M_w 5.4 and 5.6 earthquakes occurred at Lat. 66.333°N and Long. -18.805°W and at Lat. 66.299°N and Long. -18.714°W, respectively), along the GOR on 2 April 2013 (an M_w 5.4 earthquake occurred at Lat. 66.547°N and Long. -17.661°W) and on 19 February 2018 (an M_w 5.2 earthquake occurred at Lat. 66.586°N and Long. -17.708°W) (https://en.vedur.is/; Fig. 1).

A volcanic eruption occurred in Holuhraun, just north of the Vatnajökull glacier, and was part of a rifting event that originated in

the Bárðarbunga volcano (Fig. 1). The rifting event started on 16 August 2014, with a magmatic dike gradually propagating 48 km northeastward from the Bárðarbunga volcano until 27 August 2014. The dike propagation and emplacement were followed by eruptive activity beginning on 29 August 2014 and ending on 27 February 2015 (Sigmundsson et al., 2015; Andrén et al., 2016). The Bárðarbunga (dike) intrusion has been estimated ~5 m in thickness (Sigmundsson et al., 2015; Ruch et al., 2016) and it caused strain changes all over northern Iceland, as indicated by ~5 mm of GPS-determined displacements at distances beyond 100 km from the intrusion (Jónsson et al., 2019, Fig. 1).

The HA01 hydrogeochemical monitoring borehole, which is the source of the water samples analysed in this paper, is located in the Hafralækur area (Fig. 1) in a low-temperature geothermal district just south of the TFZ and ~ 20 km to the south of Húsavík (Andrén et al., 2016). In the Hafralækur–Húsavík area, the bedrock mainly consists of mafic and intermediate lavas from the Tertiary to Holocene ages with intercalated sediments (Jóhannesson, 2014). The HA01 borehole is 101 m deep and penetrates a layer of basalt-derived sediments beneath the Younger Laxá Lava, producing three lava flows (Andrén et al., 2016). From the borehole, artesian water naturally flows out after circulating into basalts and basalt-derived sediments. The borehole is cased to a depth of 35 m with filters for water inlets located at 65, 82 and 96 m, yielding a total of 7.7 L/s. The groundwater from the borehole is between 71 and 76 °C with a pH of ~10.2 (at 25 °C). The groundwater has a low dissolved solid content (240 ppm), which is typical of fresh low-temperature geothermal groundwater on the flanks of the active rift zone in Iceland (Kristmannsdóttir et al., 2010; Skelton et al., 2014, 2019; Andrén et al., 2016).

3. Data and methods

Water samples have been collected from the HA01 borehole every week from October 2008 (Skelton et al., 2019). The time window for this study is from September 2010 to June 2018. Two samples from the borehole were collected weekly to determine major (cations and anions) and trace element contents and for isotope analysis. Before sampling, to mitigate the borehole casing oxidation effects, we removed the stagnant water (shallow), then purged a fixed number of borehole volumes, generally between three to five (Trick et al., 2008). Both groundwater samples were filtered in situ through a 0.2 μm filter into acid-washed polyethylene bottles. One sample was filled leaving as little air as possible, and it was not opened again until the analysis stage. This latter sample was used for isotope analysis (Skelton et al., 2019). On the day of sampling, the sample was cooled for around one hour before pH and temperature were measured. In the second sample, Suprapur® HNO3 (Merck KGaA, Darmstadt, Germany) was added to make it 1% acidified. After a period of storage in Iceland, the samples were sent to and stored cold at the University of Stockholm and the University of Iceland in Reykjavík to analyse stable isotopes ($\delta^{18}O$ and $\delta^{2}H$) and major element concentrations, respectively (Skelton et al., 2019). Finally, the acidified water samples were sent to Rome for trace element concentration analysis (Franchini et al., 2020). This latter analysis used the same sample aliquots that had been previously analysed for the major elements (Skelton et al., 2014, 2019; Andrén et al., 2016). We measured the concentration of dissolved trace elements (lithium (Li), beryllium (Be), boron (B), aluminium (Al), vanadium (V), chromium (Cr), manganese (Mn), iron (Fe), cobalt (Co), nickel (Ni), copper (Cu), zinc (Zn), gallium (Ga), arsenic (As), rubidium (Rb), strontium (Sr), molybdenum (Mo), cadmium (Cd), indium (In), antimony (Sb), caesium (Cs), lead (Pb) and uranium (U); Table S1) at the Geochemistry Laboratory of Sapienza University of Rome with an inductively coupled plasma mass spectrometry ICP-MS (X Series 2 Thermo Fisher Scientific) (Ricolfi et al., 2020). To keep trace element stability in the solutions until analysis, in the ICP-MS laboratory, we re-checked the pH of the acidified water samples and added Suprapur® HNO_3 till to pH < 2, if needed (Marcovecchio et al., 2014). We used ultrapure water (Millipore, Milli-Q, 16 MΩ cm) to prepare blanks, standard solutions, sample dilutions and an internal standard, Rh, to correct the ICP-MS instrumental drift. The analytical accuracy of this method ranged between 2% and 5% (Barberio et al., 2017; Nigro et al., 2017). After each tenth sample, we analysed blank and two standard reference materials (SRM1640a purchased from the National Institute of Standards and Technology, United States) as water samples. The parameters for water analyses by ICP-MS (X Series II Thermo Fisher Scientific Inc.) are reported in Table S2. We measured and controlled for uncertainties for all constraints using a regular laboratory replica of samples and by confirming the precision/calibration of the instrument over regular runs with standard solutions. The recoveries of analytes of interest were in the range 98.4–106.3%, whereas recoveries of the SRM1640a were in the range 91.2–111.6%. We added 206Pb, 207Pb and 208Pb isotopes to measure the concentration of lead (Ricolfi et al., 2020).

To analyse and assess the trace element temporal series, and to avoid human influence or an arbitrary choice of anomalies, we used both Principal Component Analysis (PCA) and Change Point (CP) detection. In long-term borehole monitoring, such as for HA01, PCA is useful to identify which elements (components) and samples (loadings) deserve particular attention. After such a selection, CP detection is helpful to identify significant changes in the time-series, particularly when compared to seismic or volcanic events.

The PCA is a statistical tool that can discover unsuspected relationships that could reduce the dimensionality of the dataset while retaining the information present in the data structure. It has been successfully applied to explain the hydrogeochemical composition of geothermal waters in different geological settings (Nicholson, 1993; Boschetti et al., 2003; Awaleh et al., 2020). Different codes from OriginPro version 2019b (OriginLab Corporation, Northampton, MA, USA) and SPSS version 16 (Armonk, NY: IBM Corp; IBM, 2019) were used for classic PCA. Before PCA extraction, the sampling adequacy of the data matrix was checked for the subject-to-variables ratio (Bryant and Yarnold, 1995; Hutcheson and Sofroniou, 1999; Hatcher and O'Rourke, 2013; Garson, 2018), Kaiser-Meyer-Olkin (KMO) and Bartlett's test of sphericity (IBM, 2019). Results were also compared with categorical PCA (CATPCA) and robust PCA (RPCA) (Filzmoser and Todorov, 2013; Hubert et al., 2016). Other details are discussed below in the dedicated section.

We also used CP analysis on the temporal series of chemical data. A CP is a point in which an ordered sequence of data (y1, y2, …, yn) changes its statistical properties (Skalska, 2017). Some freely available codes can solve the detection and statistical evaluation of changes in data trends (Skalska, 2017). The Joinpoint Regression Program (JRP), version 4.8.0.1, is a software package that fits data into joinpoint models (Joinpoint Regression Program, 2020). The software enables the user to test whether an apparent change in trend is statistically significant. A sequence of permutation tests (the Monte Carlo method) identifies the CPs between trends. The procedure is based on a sequential application of likelihood ratio-type tests (Kim et al., 2000). Once the minimum (k_{min}) and maximum (k_{max}) number of CPs is set, choosing the number of statistically significant CPs is performed via a scheme of hypothesis tests that compares a simpler model, called the null model, and a more complicated model called the alternative model. This brief description does not attempt to be mathematically or statistically exhaustive; therefore, the reader is referred to the Joinpoint Regression Program (2020) for more details. In this study, we used the following operative code conditions: i) to obviate the fact that the sampling dates of the trace elements do not have regular periodicity, we used a standard error of 5% (i.e. higher than the real 2%) for each raw data concentration before elaboration; ii) we chose weighted Bayesian information criteria (WBIC) as the model elaboration, which combines both traditional Bayesian information criteria (BIC) and its modification with a harsher penalty (BIC3) using a weighted penalty term based on data characteristics (Joinpoint Regression Program, 2020). The WBIC

was considered the default in the Joinpoint software, particularly for a large dataset (N > 160 samples), because it is more computationally efficient than the permutation tests and maintains a relatively high probability of correct selection (Kim and Kim, 2016; Joinpoint Regression Program, 2020).

Concerning seismic data, we considered earthquakes from 1 September 2010 to 31 December 2018, which included ~800 seismic events ($M_w \geq 4$) in Iceland (see Fig. 1; Table S3). These earthquakes were mostly linked to the volcanic activity and caldera collapse of Bárðarbunga in 2014–2015 (indeed, these earthquakes mainly occurred between August 2014 and February 2015) and to the seismic activity of the HFF and GOR in northern Iceland (Fig. 1). All earthquake data are from the IMO catalogue (https://en.vedur.is/).

4. Results and discussion

4.1. Elemental variability of the HA01 groundwater

Before comparing the chemical data (Table S1) of the monitored HA01 borehole against the seismic and volcanic activities during this study's time window, we computed the coefficients of variation associated with HA01 groundwater trace elements in Fig. 2a (Table S4).

The coefficient of variation corresponds to the ratio between the standard deviation (σ) and the absolute value of the mean (|μ|) of results from the physical-chemical measurements and analyses realized in situ and in the laboratories on the groundwater samples collected during the considered period. The coefficient of variation is a measure

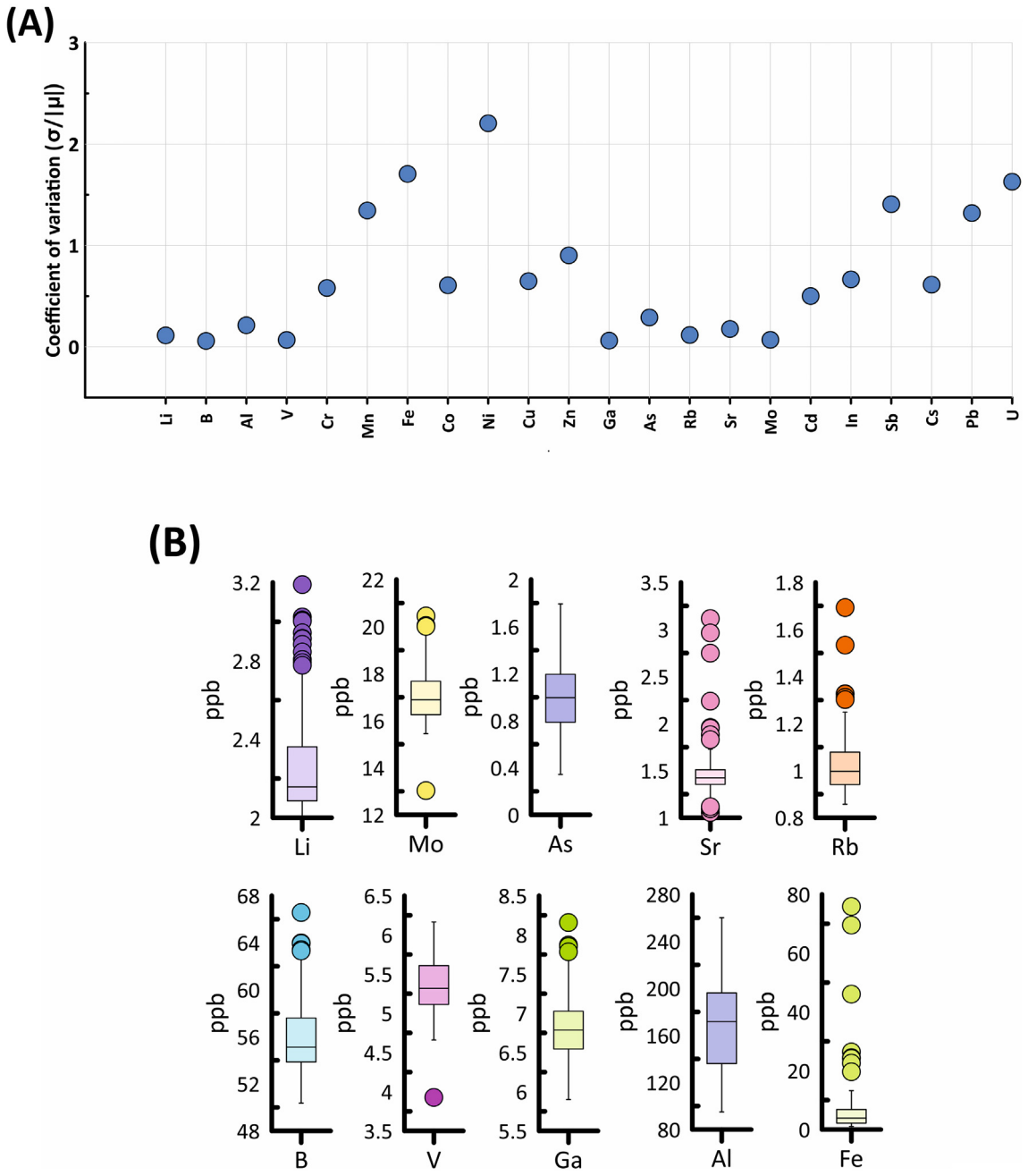

Fig. 2. Variability of elements in the HA01 groundwater. (A) Coefficients of variation for all the trace elements (Table S4). (B) Box-and-whisker plots for the selected trace elements where dots represent "anomalous values" of concentrations (ppb) compared to the median and the associated box as they exceed the whiskers.

of dispersion of a frequency distribution and shows the extent of variability in relation to the mean of the population.

The low variability range (coefficient of variation <0.5) includes Li, B, Al, V, Ga, As, Rb, Sr and Mo. The intermediate variability range (≥0.5 to <1.0) includes Cr, Co, Cu, Zn, Cd, In and Cs. The high variability range (≥1.0) includes Mn, Fe, Ni, Sb, Pb and U (Fig. 2a).

Most elements with coefficients of variation >0.5 have very low average concentrations over the sampling period, namely, less than 1 ppb or even below the quantification limit of the instrument (Table S4). For this reason, we excluded these elements (Co, Cd, In, Cs, Cr, Mn Ni, Cu, Sb, Pb, U and Zn) from our subsequent analyses and elaborations. In terms of Zn, despite an average concentration of 6.42 ppb, it was only detected in 29 out of 166 analysed samples. Although the Fe concentration was often below the instrument detection limit (in 54 samples out of a total of 166), we considered it the same because of its documented role in pre-seismic processes elsewhere (Barberio et al., 2017; Boschetti et al., 2019). The remaining elements (Li, B, Al, V, Ga, As, Rb, Sr and Mo) were mostly characterised by low coefficients of variation (<0.5), which, over a long time series (8–9 years) corroborate their suitability as good indicators for changes connected with environmental events. In other words, anomalies in groundwater concentrations are emphasised by the stability of the time series expressed by the low coefficient of variation.

To better understand the statistical distribution of the analysed populations, we also graphed concentrations of the selected elements (Li, Mo, As, Sr, Rb, B, V, Ga, Al and Fe) as box-and-whisker plots (Fig. 2b). Each box represents interquartile ranges (25–75 quartiles) and is separated into two parts by the median. The whiskers are limited by the interquartile range (IQR) with a factor equal to 1.5. All selected elements had small boxes, meaning that populations were clustered around the median. Furthermore, all elements, except As and Al, had outliers (dots in Fig. 2b), which are anomalous values compared to the median and associated box as they exceed the whiskers (Fig. 2b).

4.2. Time series of trace elements in the HA01 groundwater

The time series of previously selected (Li, Mo, As, Sr, Rb, B, V, Ga, Al and Fe) trace element concentrations (Table S1) are shown in Fig. 3. The graphic representation of the time series allowed us to appreciate the extraordinary stability found in the concentrations of Li, B, Mo, V, Ga, As, Rb, Sr and Al over nine years (Table S1), which is confirmed by the low variability of the sample around the average values (Table S1). Instead, Fe and Zn showed a very high standard deviation, which is a symptom of higher intrinsic variability and/or potential instrumental difficulties in their determination (Fig. 3 and Table S1).

Fig. 3 demonstrates that two groups can be identified based on the trends of concentration over time. The first group is represented by Li, Ga and Mo, while the second group is represented by B, V and Al. These two groups of elements exhibit similar behaviours where comparable trends of concentrations are recognised.

Sr, Rb and Fe concentrations were stable around their average values, only significantly departing between January 2018 and the end of study period (Fig. 3).

The As time series was characterised with very low and variable (but within a very narrow concentration interval of about 1 ppb) concentration values. No clear trends were visible in this narrow distribution within the monitoring period (Fig. 3).

4.3. Preliminary observations on hydrogeochemical changes vs seismic and volcanic events

To identify possible correlations between trace elements of the analysed groundwater and geological events, such as earthquakes and volcanic activity, we compared our hydrogeochemical time series with a time series of seismic events with $M_w \geq 4$ and main volcanic episodes (i.e. from the Bárðarbunga volcano) for the period of monitoring in selected areas of Iceland (Figs. 1 and 3). We identified the following possible temporal correlations:

(1) An apparent increase in B, Al and V concentrations (HA01) started about five months (May 2012) before the M_w 5.6 seismic event off northern Iceland on 21 October 2012, around 75 km from the HA01 borehole. From July 2012, the concentrations of these three elements returned to background values (Fig. 3). Different hydrogeochemical potential precursors for this earthquake were previously identified (Skelton et al., 2014, 2019; Andrén et al., 2016).

(2) From January 2014, B, Al and V exhibited a substantial decrease in their concentrations (HA01) until August 2014, when a quick inversion and increase of all three elements were recorded. This increase started about one week before the Bárðarbunga seismic sequence and rifting event (16 August 2014), which, in turn, heralded the volcanic eruption (on 29 August 2014) by about two weeks (Gudmundsson et al., 2016). Hence, the elemental inversion and increase of B, Al and V (HA01) occurred about three weeks before the Bárðarbunga eruption in Holuhraun, which occurred at around 115 km from the HA01 borehole (Bárðarbunga is located 140 km away from the borehole). Moreover, in September 2014 (after the onset of the volcanic eruption), Li, Ga and Mo concentrations started to increase. B, Al, V, Li, Ga and Mo returned to background values in February 2015 (Fig. 3).

(3) All the considered trace elements (Li, B, Ga, Mo, Sr, Rb and Fe concentrations in the HA01 groundwater), except for Al, V and As, exceeded the $+2\sigma$ threshold (Table S1) from January 2018, about seven weeks before the M_w 5.2 earthquake off northern Iceland on 19 February 2018, approximately 70 km from the HA01 borehole (Fig. 3). Concentrations of these elements remained high until the end of our study period (June 2018).

(4) Some hydrogeochemical variations occurred in 2016–2017 (HA01) when no significant seismic and volcanic activities occurred. In particular, Li, Ga and Mo exhibited a substantial increase in groundwater concentration (HA01) from December 2016 to November 2017, whereas B, Al and V exhibited a substantial increase from January to June 2017 (Fig. 3). In the same period, the concentration of some major chemical elements in the HA01 water showed anomalous changes (Skelton et al., 2019).

The aforementioned potential correlations between hydrogeochemical trends and seismic-volcanic events are statistically tested below.

4.4. Trace element hydrogeochemistry and volcanic events

As mentioned above and observed in Fig. 3, hydrogeochemical changes before the 2014 Bárðarbunga activity were the most obvious over the recorded time series. We propose some geochemical-thermodynamic computations to understand the possible sources of trace elements (and their pre-volcanic concentration changes) in Icelandic volcanic environments.

Earthquakes are among the most important signals in forecasting eruptions because magma movement enhances the stress of the surrounding rocks. However, seismic activity in volcanic areas can be characterised with wide variability depending on the large range of elastic behaviour and rheology of the rising magma and surrounding rocks (Marzocchi and Bebbington, 2012). Among the main volcanic precursors, geochemical signals may be important in forecasting volcanic eruptions (Marzocchi and Bebbington, 2012). Monitoring methods based on chemical changes related to volcanic activity have been used to detect changes within the volcanic system. Geochemical monitoring has mainly focused on gas emissions from fumaroles or craters and, less frequently, the studies have addressed changes in remote groundwater geochemistry before volcanic eruptions (Armienta et al., 2008).

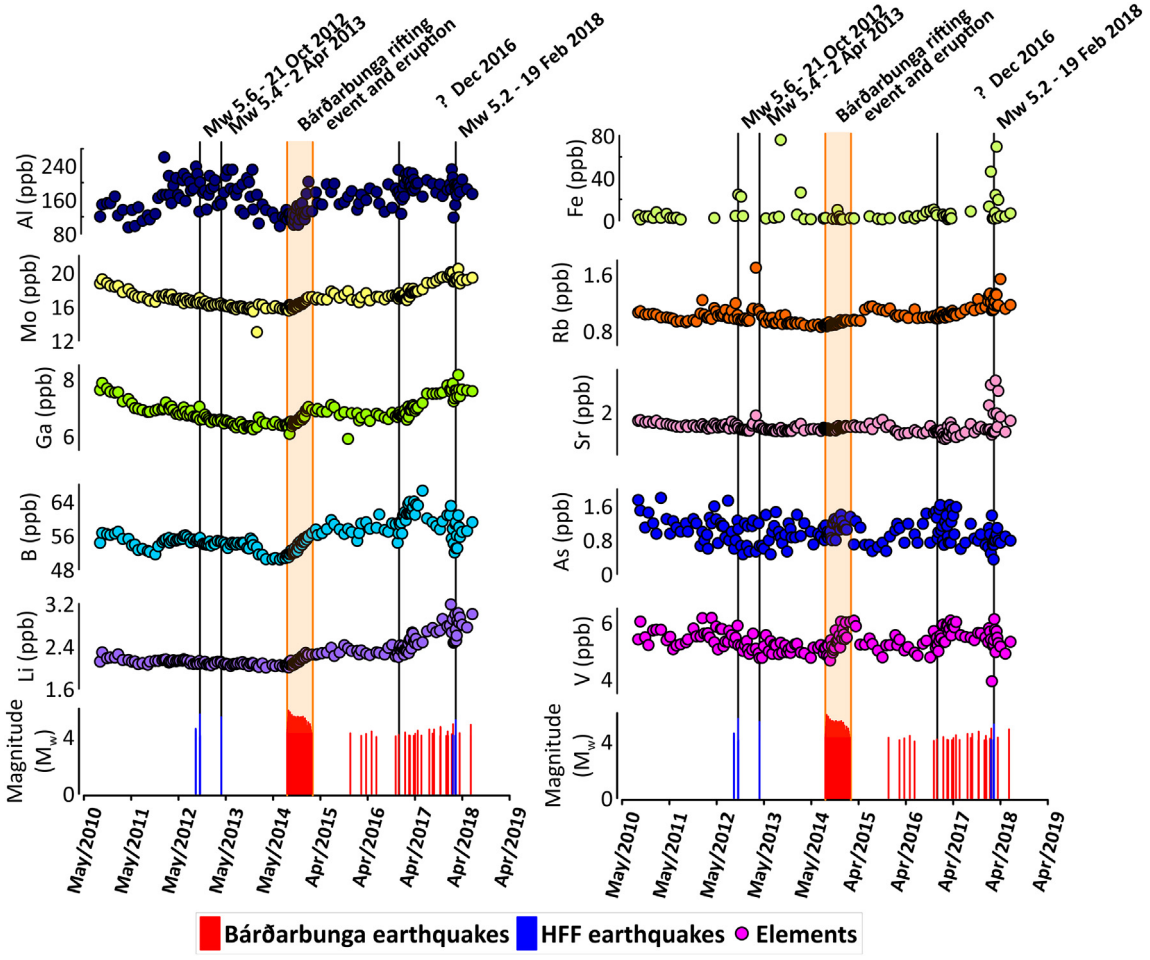

Fig. 3. Time series of trace element concentrations and major earthquakes and volcanic eruptions. Trace elements concentrations in the HA01 groundwater (ppb; September 22nd, 2010 – June 25th, 2018; Table S1) are shown with circles of different colors. Seismic events ($M_w \geq 4$; January 13rd, 2011 – February 23rd, 2019; Table S3) related to the Bárðarbunga Volcano and Húsavík-Flatey Fault (HFF) activities are displayed with red and blue bars, respectively. Earthquake data are from the IMO catalogue (https://en.vedur.is/). (For interpretation of the references to color in this figure legend, the reader is referred to the web version of this article.)

Nonetheless, the application of geochemical monitoring methods to water (springs, streams, etc.) associated with volcanism has proven to be productive in understanding mechanisms related to volcanic activity (Armienta and De la Cruz-Reyna, 1995). In an active geothermal system, as is this case study in Iceland, fluids can remotely transport or deposit metals that originate from source water, magmatic volatiles and via rock dissolutions (Kaasalainen et al., 2015; Blomgren et al., 2019). For example, B is highly mobile during water–rock interaction in a basaltic-hosted geothermal system and, therefore, is a good indicator of rock leaching. B is a chemical species that is more sensitive to changes in volcanic activity. Indeed, magma displacement can lead to dome or dike emplacement facilitating the leaching of the host rock. For this reason, the hydrogeochemical composition of springs varies with the changes in volcanic stress pattern (Armienta et al., 2008; Arnórsson and Andrésdóttir, 1995; Kaasalainen et al., 2015).

The calculation of the trace elements' relative mobility (Gislason et al., 1996; Aiuppa et al., 2000; Koh et al., 2016), i.e. the normalised-to-sodium ratio between the trace concentrations detected in the HA01 borehole and basalt (Kokfelt et al., 2006; Kaasalainen and Stefánsson, 2012; Shorttle et al., 2013), definitively confirms that B is the most mobile element in the studied area (Supplementary File RM). Therefore, to examine the volcanic hydro-sensitivity of B, we analysed the relationship between B and trace element concentrations in the geothermal aquifer fluids of the Hafralækur area (Fig. 4). We compared our water samples (black dots) with data from previous studies on snow samples from the Vatnajökull glacier and highland NE of the glacier during the 2014–2015 Bárðarbunga eruption (white rhombuses; Galeczka et al., 2017), water samples from the Jökulsá á Fjöllum River (JFR) during the 2014–2015 Bárðarbunga eruption (light blue squares; Galeczka et al., 2016), Icelandic cold groundwater (green triangles; Kristmannsdóttir and Klemensson, 2007; Kristmannsdóttir et al., 2009; Kristmannsdóttir, 2011) and Icelandic thermal groundwater (orange triangles; Arnórsson, 1969; Kristmannsdóttir and Klemensson, 2007; Kristmannsdóttir, 2008; Kristmannsdóttir et al., 2009; Kristmannsdóttir, 2011; Kaasalainen and Stefánsson, 2012; Kaasalainen et al., 2015). The transition temperature between cold and thermal waters was 10 °C (Kristmannsdóttir and Klemensson, 2007; Kristmannsdóttir et al., 2009; Kristmannsdóttir, 2011), in agreement with Schoeller's (1962) definition of thermal waters (air or surface water temperature over 4 °C). In Húsavík, the mean annual temperature of surface water was approximately 5.6 °C, and the transition between cold and thermal waters occurred at around logB = 1. The logarithmic values tended to fade the temporal element variability, particularly in samples with a lower coefficient of variation values. However, it was possible to have some indication of the origin of the trace constituents by comparing them with the concentration of median trace elements in Icelandic basalts (Kaasalainen and Stefánsson, 2012) and with the data from Icelandic thermal waters at temperatures lower than or equal to 100 °C (Arnórsson, 1969; Kaasalainen and Stefánsson, 2012; Kaasalainen et al., 2015). Geochemical-thermodynamic codes can be used to model the equilibria of major and trace elements during water–rock interaction (e.g. reaction-path modelling; Marini, 2013; Kaasalainen et al., 2015). However, the low concentration of trace

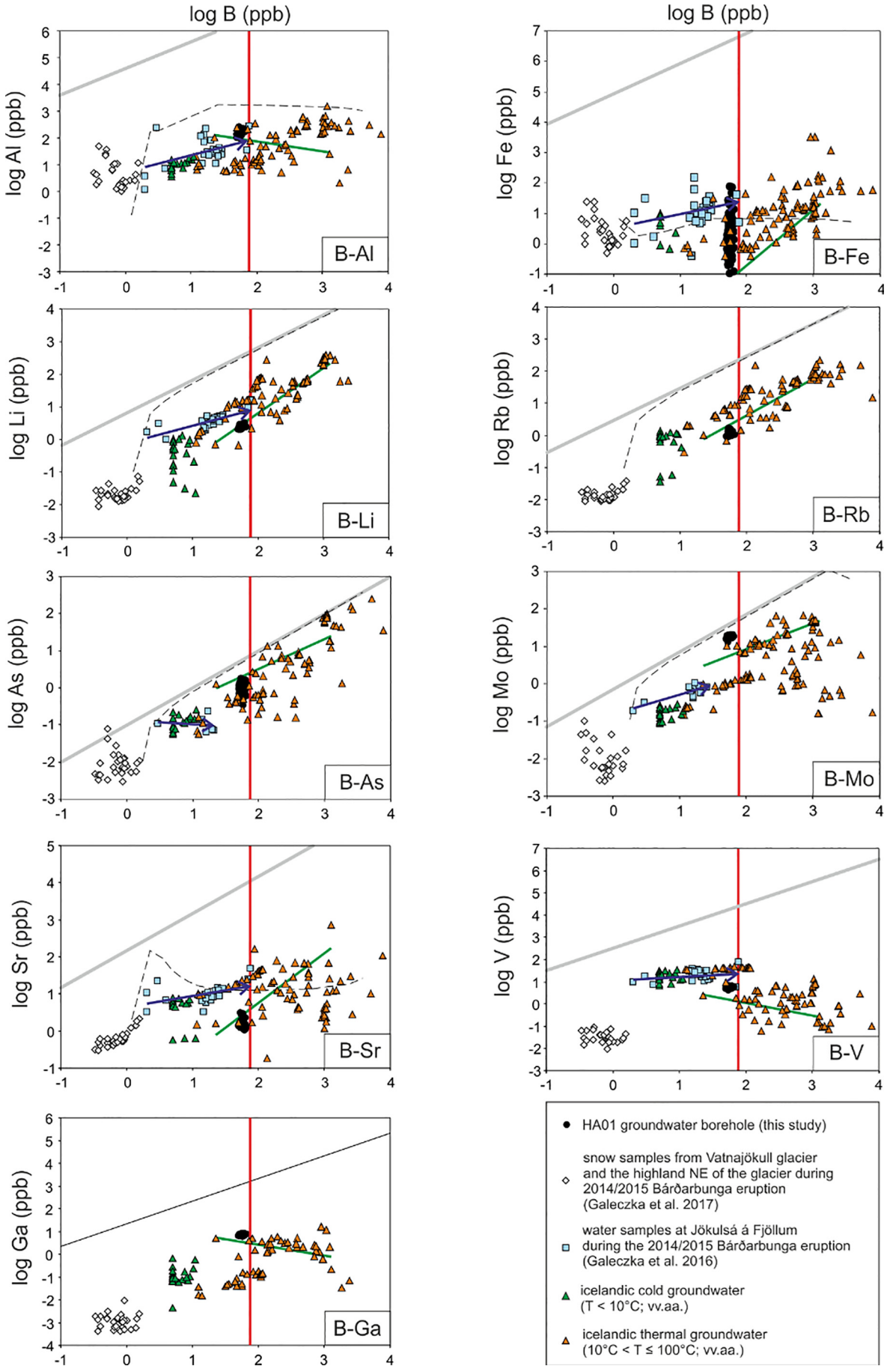
log B (ppb)
log Al (ppb)
B-Al
log Fe (ppb)
B-Fe
log Li (ppb)
B-Li
log Rb (ppb)
B-Rb
log As (ppb)
B-As
log Mo (ppb)
B-Mo
log Sr (ppb)
B-Sr
log V (ppb)
B-V
log Ga (ppb)
B-Ga
HA01 groundwater borehole (this study)
snow samples from Vatnajökull glacier and the highland NE of the glacier during 2014/2015 Bárðarbunga eruption (Galeczka et al. 2017)
water samples at Jökulsá á Fjöllum during the 2014/2015 Bárðarbunga eruption (Galeczka et al. 2016)
icelandic cold groundwater (T < 10°C; vv.aa.)
icelandic thermal groundwater (10°C < T ≤ 100°C; vv.aa.)

elements in T ≤ 100 °C groundwater combined with the difficulty in taking other phenomena into account, such as adsorption/absorption in minerals (in particular oxides and hydroxides), co-precipitation in complex phases (such as the solid solutions or mixed layered clays) and the incompleteness of the thermodynamic data on solution species, mean that these models must be used with extreme caution when applied to trace elements (Oelkers et al., 2009; Marini, 2013). This is evident in Fig. 4, especially in the case of Li and Rb, where the borehole waters were positioned below the reaction path model created by Kaasalainen et al. (2015). That model was calculated for high-temperature geothermal waters in Iceland; however, the first stretch of the path (low B content) can be compliant for waters at T ≤ 100 °C, as in the case of the HA01 borehole. It is relevant to observe how the HA01 samples are clustered at the switch domain between the surface waters of JFR (Galeczka et al., 2016) and Icelandic thermal waters, which are approximated by the maximum boron content detected in JFR during the 2014–2015 Bárðarbunga eruption (logB = 1.8) (Fig. 4). The samples tend to be closer to the reaction path model in the case of Sr, Al and Fe, with the first one being quite immobile compared to boron. The HA01 borehole groundwater samples have lower contents in Sr compared to the reaction path model and Icelandic thermal waters, probably due to the high pH of the HA01 groundwater (i.e. faster calcite precipitation especially close to the surface conditions) and/or co-precipitation in calcic zeolites (Andrén et al., 2016).

The Al and partial Fe concentrations in HA01 groundwater align with the trend of JFR samples towards Icelandic thermal waters. These two elements are geochemically similar and can be classified as immobile trace elements (Supplementary File RM), probably due to their tendency to form oxide-hydroxide colloids. However, Fe has the greatest variability in the parity of B concentration, probably due to variable redox conditions and/or the fact that iron resides in the structures of nano- to micron-scale clay mineral particles undergoing cycling between Fe(II) and Fe(III) (Ilgen et al., 2019). In contrast, Mo is the second more mobile trace element after B (Supplementary File RM). Its concentration in the HA01 groundwater is also noteworthy because, similarly to basalts, it is much higher than in surface waters and slightly shifts towards higher concentrations compared to other Icelandic thermal waters (Fig. 4). Mo does not have a very high basalt concentration, but it tends to accumulate in water proportionally to the time and temperature of interaction (Arnórsson and Óskarsson, 2007). This confirms that the HA01 groundwater is ancient and probably originated from glacial melting; it is roughly datable to the pre-early Holocene era as suggested by the low stable isotope ratio value of hydrogen, $\delta^2H(H_2O)$ (Skelton et al., 2014). Therefore, it is clear that the analogy of the B content between JFR waters and the HA01 borehole before and during the 2014–2015 volcanic crisis is a mere coincidence, even if the position of the borehole on the growth trend of the trace elements in the water is compatible with its origin from glacial melting. Indeed, in Iceland, early Holocene (12–8.2 cal ka) deglaciation and pulsed warming were associated with two major generations of *jökulhlaups* (glacier outburst mega-floods) around the Vatnajökull icecap at 11.4–11.2 cal ka and 10.4–9.9 cal ka and major tephra emissions from the Grímsvötn and Bárðarbunga subglacial volcanoes (Van Vliet-Lanoë et al., 2020).

We indicated the evolution of the JFR during the 2014–2015 event (purple arrow) along with a less-marked line representative of the correlation of the samples typical of the thermal waters of north Iceland (among which there is also the HU01 borehole; Kristmannsdóttir, 2008) (Fig. 4). As well as the HA01 borehole, these samples have a more basic pH (median equal to 9.7) compared to the others (8.37 in Kristmannsdóttir and Klemensson, 2007; Kristmannsdóttir et al., 2009; Kristmannsdóttir, 2011; 8.66 in NaCl waters in Kaasalainen and Stefánsson, 2012). It is noteworthy that basic pH values are typically measured from water originating from glaciers and are caused by the isolation of groundwater atmospheric CO_2 (Vigier et al., 2006). The correlation line (green line) is always close to the HA01 samples (Fig. 4). Therefore, this line can be representative of the evolutionary trend of the waters in the Hafralækur area. However, water samples from the HA01 borehole represent the transition between JFR and thermal waters (vertical red line) that are especially evident in the Al and Fe graphs. Moreover, trends of HA01 and other basic samples are similar for elements with geochemical affinities, such as Al and Ga (different mobility but with a similar dissolved species behaviour due to the pH; Elmi, 2009), As and Mo (similar high mobility and affinity with sulphides) and Li and Rb (similar moderate mobility and parallel trend to the ratio B/alkali metal in basalts) (Fig. 4; Supplementary File RM). Finally, the concentration of alkali metals Li, Rb and Cs in geothermal fluids increased with increasing temperature (Kaasalainen et al., 2015). This also explains why the trend is different from the high-temperature geochemical model (dotted line), given that the HA01 borehole has a deep T equal to ca. 100 °C (Fig. 4). In Fig. 5, most of the HA01 borehole samples are clustered between the mean composition of meteoric water and a Li/Rb = 2.26 weight ratio, which is between that of basaltic glass (Li/Rb = 2.33 in Berger et al., 1988, which is also similar to MORB, Li/Rb = 2.26 in Gale et al., 2013) and the median ratio of Icelandic tholeiitic basalts (Li/Rb = 2.18; Kaasalainen and Stefánsson, 2012), the latter also being enriched with more Cs (Fig. 5). Generally, processes related to the distribution of these elements in thermal waters are particularly evident at high temperatures in the following range: 150 < T < 350 °C (Seyfried Jr and Bischoff, 1979; Seyfried Jr., 1987; Giggenbach, 1991; Kaasalainen et al., 2015). In such a temperature range, the absorption of Li on quartz or Cs on zeolites is more pronounced (Giggenbach, 1991).

The calculation of the relative mobility of trace elements confirms that B is highly mobile during water–rock interaction in a basaltic-hosted geothermal system (Supplementary File RM). In particular, the analysis of the relationship between B and trace element concentrations in the geothermal aquifer fluids of the Hafralækur area allows us to confirm that water samples from the HA01 borehole represent the transition between JFR and thermal waters (Fig. 4). Furthermore, the noteworthy concentration of Mo confirms that the HA01 groundwater is ancient, probably originating from glacial melting and roughly datable to early Holocene (Arnórsson and Óskarsson, 2007; Skelton et al., 2014).

4.5. Principal Component Analysis (PCA)

In this study, some previously investigated major constituents such as Ca, Na, Si and K (Skelton et al., 2014, 2019) were added to the trace element database (Li, B, Al, V, Ga, As, Rb, Sr, Mo) to elicit as much information as possible from PCA. This addition also helped compensate for the lack of some trace elements that were not considered in PCA processing as they were below the quantification limit. A data matrix of 13 variables (the elements) and 156 subjects (the samples) was obtained that agreed with the subject-to-variables ratio of Bryant and

Fig. 4. Relationships between B and trace element concentrations in the HA01 groundwater. Solid black line depicts the boron/element ratios according to Kaasalainen and Stefánsson (2012, and references therein), except for Ga (median Ga value from Arnórsson, 1969; De Argollo and Schilling, 1978; Willis, 1979; Reimann and De Caritat, 1998). Purple arrow shows the trend line of the trace elements in the Jökulsá á Fjöllum River samples (white squares) during 2014–2015 Bárðarbunga eruption (Galeczka et al., 2016); vertical red line shows the maximum boron concentration detected in the river during that period (log B = 1.8). Snow samples during the same periods are also shown for comparison (white diamonds; Galeczka et al., 2017). Dashed lines depict the reaction-path modelling for high temperature geothermal water (meteoric water – basalt interaction at 260 °C; Kaasalainen et al., 2015). Green and orange triangles are Icelandic cold (T < 10 °C) and thermal waters (10 °C < T ≤ 100 °C) (see the main text for a complete reference list), respectively; green line depicts the best fit of high-pH thermal waters in northern Iceland. (For interpretation of the references to color in this figure legend, the reader is referred to the web version of this article.)

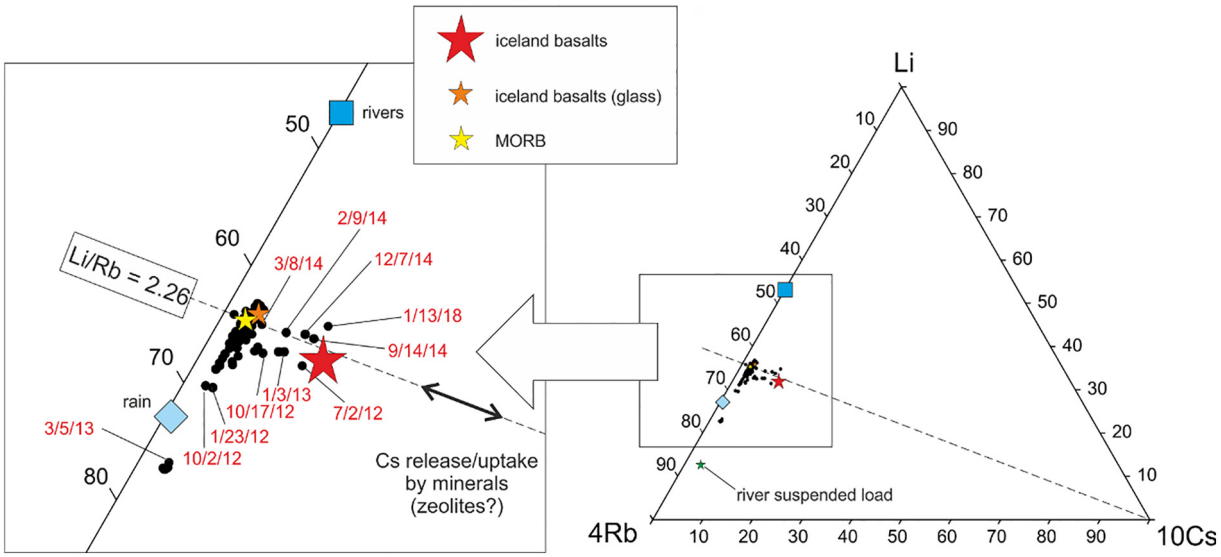

Fig. 5. Li-Rb-Cs ternary diagram. Element percentage from ppb (waters) or ppm (rocks) concentration values are reported over the diagram sides. Black dots show HA01 borehole monitoring trace dataset (this work, Table S1; Li/Rb = 2.26 is the median value of that dataset). Median basalt (Kaasalainen and Stefánsson, 2012), basaltic glass (Berger et al., 1988), MORB (Gale et al., 2013), river and rain waters (Kaasalainen and Stefánsson, 2012) are also shown for comparison. Black dots with sampling date labels as MM/DD/YY.

Yarnold (1995), STV > 5 and other rules of thumb related to the dimension of the subjects (Garson, 2018): subjects = variables x 5 or subjects >100 (Hatcher and O'Rourke, 2013); subjects >150 (Hutcheson and Sofroniou, 1999). The principal components were extracted using the correlation matrix in OriginPro code (Supplementary File 1). Similar results were obtained using the SPSS code, which had the additional option to rotate the extracted components using Varimax (IBM, 2019). With this latter code, both the KMO measure of sampling adequacy (KMO = 0.746) and Bartlett's test of sphericity (significance level ≪ 0.05) indicated that PCA was useful for interpreting the dataset. As suggested by the scree plot's elbow, the right number of components was four, which explains 75% of the cumulative variance of the data (OriginLab, 2019; Supplementary File 1). However, considering that the variance associated with the fourth component (PC4) was less than 10% and that the third component (PC3) was mainly associated with one trace element (As; see the 3D vector plot of the first three components in Supplementary File 1), the PCA results were interpreted using a binary plot, which shows both the variable eigenvectors and the PC1 and PC2 scores related to the samples (Fig. 6). In that plot, As is represented on the centroid of the diagram. Three main associations of the other variables are evident: i) a correlation between Na and Si vectors mainly represented by the positive side of PC2 (Y-axis); ii) the relationship between K and Ca vectors oriented towards the negative quadrant of Fig. 6; iii) the grouping of the trace elements' vectors on the positive side of PC1. Moreover, the sample scores showed a counter-clockwise distribution starting from 2010 (up/right quadrant, Y-axis, PC2). After that, the 2012–2013 samples are distributed just above the positive side of PC2, which is mainly represented by Na and Si variable vectors. This pattern agrees with the chemical variations detected during the swarm events of that period (Skelton et al., 2014), which were related to the labradorite–analcime reactions reported in Andrén et al. (2016). The subsequent clustering of the samples is on the negative (left) side of PC1, which seems to be related to a period of lower chemical concentration of most trace elements described by PC1 (from June 2013 to June 2014). After that, the chemical variability of samples collected in the second half of 2014 progressively shifts towards the K vector. In particular, the samples collected after the seismic swarms at the Bárðarbunga volcano (August 2014) seem not only related to that seismic event but also to the heat flow variations in that area (Reynolds et al., 2019). Indeed, the November 2014 samples, which correspond to the maximum thermal power in the cauldrons produced by new magma inflow in the volcanic system (Li et al., 2021; Reynolds et al., 2019), are exactly at the top of the K vector (Fig. 6; Supplementary File 2). The samples collected from late 2014 to late 2017/early 2018 migrate gradually towards the lower right quadrant near the apex of the B and Li vectors and subsequently, towards the upper-right quadrant of Fig. 6 (January/February 2018). This might be related to post-eruptive changes after the Bárðarbunga-Holuhraun rifting event (Li et al., 2021; Reynolds et al., 2019). Accordingly, the time-series variation of the deep temperatures inferred by Na/K (Verma and Santoyo, 1997) and Na-K-Ca (Fournier and Truesdell, 1973; Fournier and Potter II, 1979; Fournier, 1989) geothermometric equations applied to the HA01 samples show a maximum temperature at the end of 2014 and other minor jumps in the second half of 2016 (Supplementary File 3). Finally, the progressive temporal shifting of the samples towards the trace element vectors mainly related to the positive side of PC1 (Fig. 6) agrees with the fact that the pre-seismic/seismic events related to 2018 (i.e. the M_w 5.2 earthquake on 19 February 2018) are detectable only with trace elements.

A second PCA used the correlation matrix of the trace elements and aimed to better interpret their behaviour. The KMO (0.721) and Bartlett's test (significance level ≪ 0.05) results certified once again the suitability of the data for structure detection. The main characteristics of this analysis are i) the two main components that explain the 60% of cumulative variance confirm the V, B, Al and Li, Ga, Mo clustering mentioned in the previous section (the latter group is mainly explained by the PC1 axis); ii) at the extreme of the negative side of PC1, samples collected before the Bárðarbunga eruption are grouped, confirming their concentration decreased before the event; iii) on the opposite side of PC1, early 2018 samples are well distinguished as outliers not only by Li, Ga and Mo but also by Rb. The samples collected during the 2012–2013 seismic swarms are indistinguishable from the others because they fall in the centroid of the diagram, confirming that the seismic events during that period are not highlighted by trace elements. Considering that PC1 explains most of the cumulative variance, it could be used as a single variable encompassing all trace elements and reducing unnecessary background information. Both the Varimax rotation and alternative methods of component extraction, such as CATPCA (Ma et al., 2016) or RPCA (Jung et al., 2014), do not increase either the percentage of variance explained by PC1 or the discrimination capacity of its scores (Supplementary File 4). Indeed, it is evident that the scores related to PC1 extracted by classic PCA have a higher peak close to the

date of the 2014 Bárðarbunga eruption and a lower peak in late 2017/early 2018 events compared to those obtained by Varimax-rotated, CATPCA or RPCA (Supplementary File 4).

In summary, the PCA indicates that the seismic events during 2012–2013 were not preceded by significant changes in trace element concentrations, while the 2018 seismic event was preceded by only trace element changes, but not by major element changes. Furthermore, the chemical variability of the groundwater samples collected after the pre-eruptive seismic swarm of the Bárðarbunga volcano (August 2014) is not simply related to seismic events but rather might be connected to post-rifting changes after the Bárðarbunga-Holuhraun rifting event (Reynolds et al., 2019).

4.6. CP detection in the time series

Change Point (CP) detection in the time-series data of the six trace element clusters detected by the PC1 axis (B, Al, V, Li, Ga and Mo; Fig. 7) reveals that each cluster has at least one CP within a central period, which is characterised by seismic events that occurred before and during the Bárðarbunga eruption (Fig. 7; Supplementary File CP). Compared to the first earthquake, the main eruption and following seismic events in the period marked by CPs have a broader date range. The dates marked by CPs span from 10 November 2013 for Al until 22 November 2015 for Ga, with the start of pre-volcanic seismicity (16 August 2014) and eruptive events of the Bárðarbunga (29 August 2014) approximately in the middle of the time series (Fig. 7). The CPs of Al should be taken with caution because it is an element with low mobility. However, the first Al CP is followed by a CP in boron (the most mobile of all trace elements) on 1 December 2013, which marks the beginning of a declining trend in concentration, which then reverses on 8 March 2014. Element by element, it is difficult to explain the causes of these variations. However, it is interesting to note how the first CPs coeval with the stress accumulation detected in the north Iceland BRE seismic station, which is located immediately above the fault-plane of the Húsavík-Flatey transform fault, and it monitors shear-wave splitting (Hong et al., 2020). At BRE, the stress accumulation connected to the Bárðarbunga event was related to the overpressure of the microfractures' fluid, which began in August 2013, a year before the first pre-volcanic seismic shock at Bárðarbunga (Hong et al., 2020). Therefore, the first detected CPs described here could be linked to fluid overpressure in the microfractures before the main seismic event. In contrast, we speculate that late thermal variations connected to the Bárðarbunga eruption, which persist until the end of 2015 (Reynolds et al., 2019), may have been marked by the CPs of V and Ga, K in the PCA (Fig. 7) and geothermal analysis using the main chemical constituents as described in the previous section.

The second period, characterised by at least one CP in all elements except Ga, is positioned just before the M_w 5.2 earthquake on 19 February 2018 (Fig. 7). Before that seismic event, mobile elements had two (Mo) or three (B, Li) CPs. In particular, after an increasing trend, B starts to decline in concentration on 23 April 2017, approximately one month earlier than the other elements. Then, both B and Li start an abrupt decline on 1 January 2018, followed by an increase on 3 February 2018, i.e. two weeks before the seismic event. It should be noted that the alkali elements ternary diagram (Fig. 5) also shows an outlier on 13 January 2018. The precursor trends and related CPs, although not supported by all trace

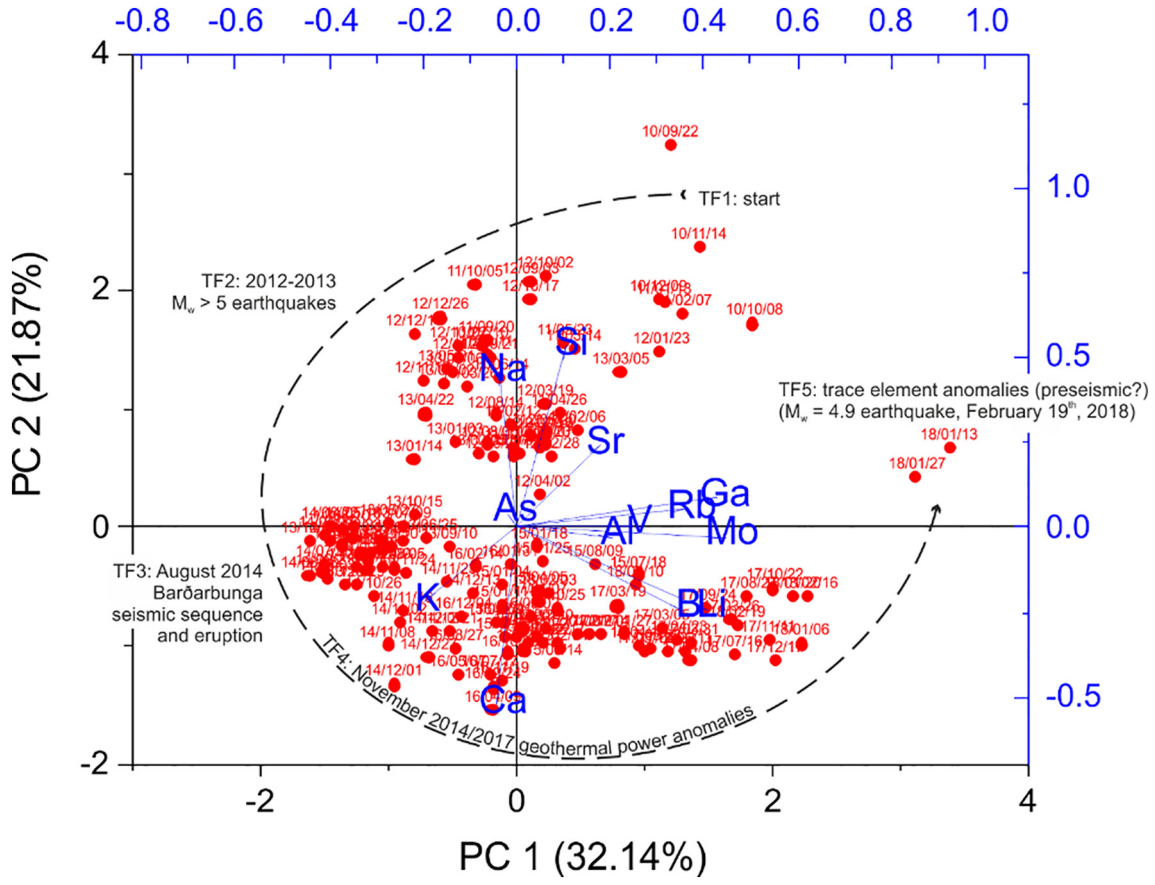

Fig. 6. Principal Component Analysis (PCA) plot. Both the loadings of the variables (eigenvectors, in blue) and the scores assigned to the sampling points (red dots with sampling date labels as YY/MM/DD) are shown, in relation to the first two component (PC1 and PC2). Preliminary data (e.g., correlation matrix) and full results of the PCA are in the Supplementary File 1. The dashed curve depicts an approximated temporal evolution path of the distribution of the sample scores, which seems marked by 5-time frames (TF#). A closer look to the diagram is reported in the Supplementary File 2, showing a magnification of time frames and labels of the sampling data. (For interpretation of the references to color in this figure legend, the reader is referred to the web version of this article.)

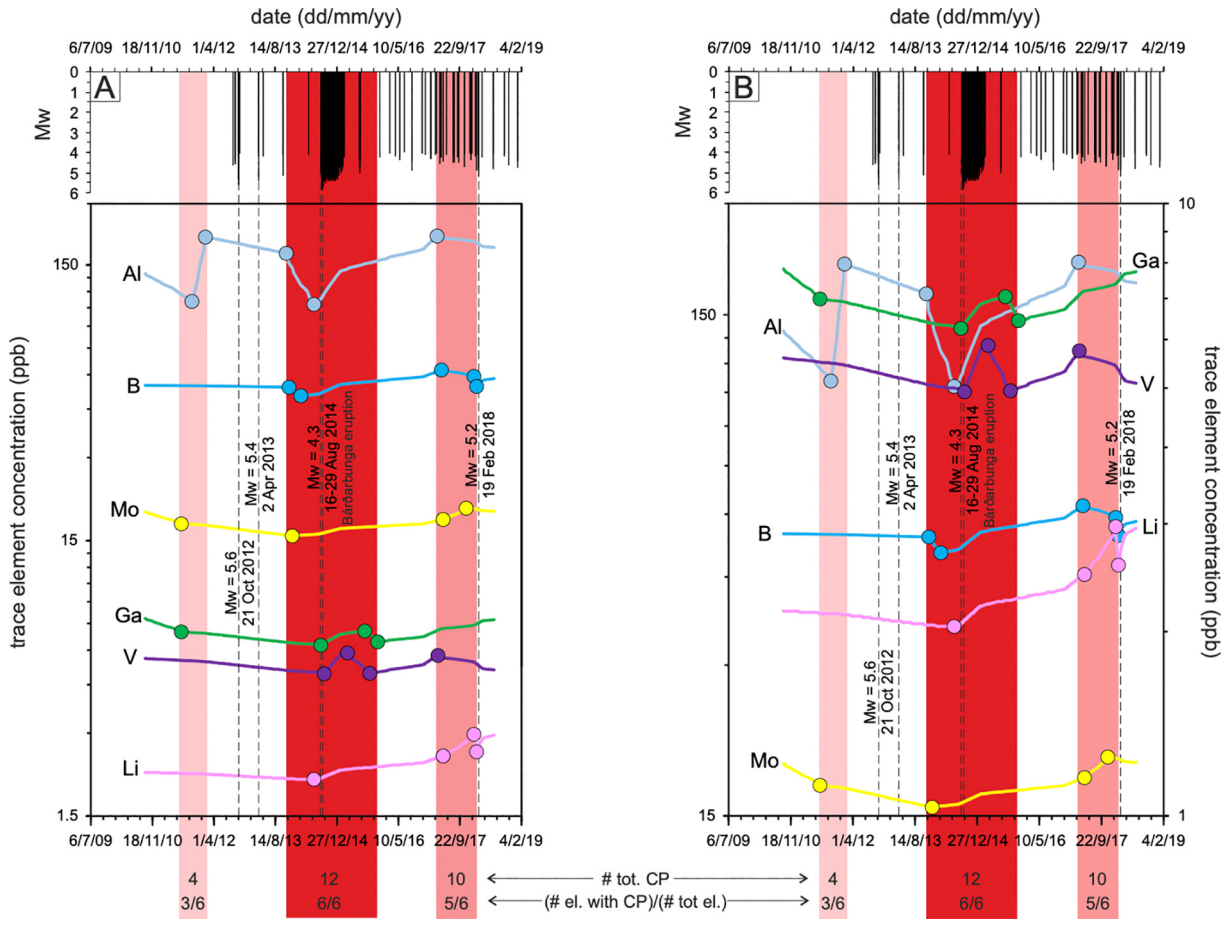

Fig. 7. Change Point (CP) diagram. Comparison between earthquake dates (top of the diagrams, vertical black bars and dashed lines; magnitude moment scale Mw) and the statistically significant change points (CPs) and trends analysed by the JRP code (colored circles and paths, respectively; Joinpoint Regression Program, 2020) related to the six elements clustered on PC1 (Al, B, Ga, Li, Mo and V). In (A), the ppb concentration scale of the elements is referred to the left $\log_{10}$ axis. In (B), to better show the slope of each element trend between the CPs, the elemental concentration within the first decade was splitted to the secondary axis on the right. Along the paths, elbows not marked by circles are statistically not-significant variations in the trends. In both diagrams, the vertical periods shaded in red highlight three different time frames having a different density of change points (bottom of the diagrams): the greater the number of change points (# tot CP) or the elements with CP to the total (# el. CP/6), the darker the red tone. (For interpretation of the references to color in this figure legend, the reader is referred to the web version of this article.)

elements (5–6), could be due to a more significant role of water–rock interaction, particularly in the different solubility and chemical composition between the glass and crystalline phase of the rock (Fig. 5) or because of the role of adsorption/desorption carried out by the secondary mineral phases in the aquifer fractures (clays, zeolites).

Finally, Mo and Ga have a CP on 10 July 2011, while Al shows two CPs, the first on 5 October 2011 and the second on 23 January 2012 (Fig. 7). As they are not confirmed by other highly mobile elements, such as B and Li, the supposed time frame has a low significance or low probability (4 CPs in 3/6 elements; Fig. 7). This was confirmed by PCA, which did not find any structure in the trace element data of that period (Fig. 6). From October 2008 to September 2012, abrupt changes were detected in $\delta^{18}O$, accompanied by steadily decreasing concentrations of the main constituents (Na, Si, Ca) (Skelton et al., 2014). These were connected to a progressive decrease in the proportion of groundwater affected by water–rock interaction (Skelton et al., 2014). Therefore, in the absence of a better explanation of their origin, these CPs could be classified as false positives or not directly related to seismic events.

4.7. Pre-eruptive and pre-seismic hydrogeochemical changes: a closer look at the results obtained by statistical analyses

The hydrogeochemical changes recorded before and immediately after the onset of the 2014 Bárðarbunga eruption are the most evident over the recorded time series (Fig. 3); this is also demonstrated in the PCA and CP statistical analyses (Figs. 6 and 7, respectively). In particular, B and Al concentrations show significant decreases, and Mo has a flattening trend due to its stable concentration from eight months before the Bárðarbunga eruption (Fig. 7). Later, the same elements start to increase in concentration before the rifting event and the following volcanic eruption. Moreover, Li, V and Ga concentrations recorded a similar temporal pattern, with the inversion of concentrations occurring circa two months (Li) or one day (Ga) before the start of the rifting event and one month (V) after it (Fig. 7). We interpret these hydrogeochemical signals as connected with the large Bárðarbunga rifting event and eruption and, therefore, the changes in B, Al, Mo and Li, V, Ga concentrations are considered as potential remote volcanic precursors.

As mentioned above, previous studies documented the hydrogeochemical sensitivity to earthquakes of the HA01 borehole groundwater, at least for some major constituents (mainly Na and Si) and stable isotope ratios of water molecules (Skelton et al., 2014, 2019). In this study, neither PCA nor CP analyses detected significant concentration anomalies or trend variations in trace elements before and after the 21 October 2012 M_w 5.6 seismic event.

In contrast, pre-seismic hydrogeochemical changes occurred before the M_w 5.2 earthquake on 19 February 2018. All the considered trace elements (Li, B, Ga, Mo, Sr, Rb and Fe) significantly increased their groundwater concentrations from about seven weeks before the earthquake

(Fig. 3). A similar element clustering and increasing trend marked by significant CPs have been statistically demonstrated by PCA and CP analysis, respectively (Figs. 6 and 7). It is noteworthy that no major chemical elements or stable oxygen–hydrogen isotope ratios of water (i.e. $\delta^{18}O$ and $\delta^{2}H$) significantly changed their groundwater concentration before this earthquake (Skelton et al., 2019). This evidence is a significant clue that trace elements may be hydrogeochemically sensitive to pre-seismic crustal deformation, particularly for intermediate magnitude earthquakes, such as the one occurred on 19 February 2018 in northern Iceland (M_w 5.2). Further evidence is necessary in the future to support or refute this idea because, in the case of the 2013 M_w 5.4 earthquake, pre-seismic hydrogeochemical anomalies in major element concentrations were recorded (Skelton et al., 2014; Andrén et al., 2016; Skelton et al., 2019), whereas any anomaly in the same samples regarding trace elements was found (Fig. 3). The deviation from the equilibrium between labradorite and analcime was invoked by Andrén et al. (2016) to explain Na and Si variations during the 2012–2013 seismic events. This process was triggered by a new input of Holocene groundwater (Skelton et al., 2014, 2019), which probably had lower trace element content than the two other members involved in the mix (pre-Holocene meteoric water and an ^{18}O-enriched component due to interaction with fresh basalt; Skelton et al., 2014). Therefore, the variations in the stable isotope ratios documented before the 2012 earthquake (Skelton et al., 2014) and the generalised and smoothed decrease in trace element concentration (Fig. 3), but marked by Al, Mo and Ga CPs during July 2011 (Fig. 7), are probably related to these hydrological/permeability changes. Indeed, it should be noted that the depleted ^{18}O-water component that was affected by water–rock interaction showed a significant input from April 2011 to May 2012 (Fig. 3b in Skelton et al., 2014). The geochemical relationship between Al and Ga, also highlighted by similar trends in Fig. 7, and the fact that Mo is not concentrated in a modern-day groundwater component has already been underlined.

On the contrary, significant pre-eruptive anomalies in the trace elements were recorded during 2014 (Figs. 6 and 7) without significant anomalies concerning major elements (Skelton et al., 2014, 2019). The complex role and sensitivity of potential hydrogeochemical precursors, the role of influencing factors, such as type, distance and magnitude of the causative geological events (e.g. earthquakes, volcanic eruptions) and the subsurface geological setting (site-specificity) indicate that we are only at the beginning of understanding this process.

Our interpretation of the recorded hydrogeochemical changes as potential seismic or volcanic precursors is questioned by the observation that, in 2016–2017, some hydrogeochemical variations occurred when no significant seismic and volcanic activities were recorded. In particular, two elemental triplets (Li, Ga, Mo and B, Al, V) exhibited a substantial increase in groundwater concentration during this time (Fig. 3). PCA demonstrated that the grouping of trace elements with K that occurred from late 2014 to late 2017/early 2018 could be related to the thermal phase that marked the transition between the post-eruptive phase of the Bárðarbunga and the seismic event that occurred during 2018 (Fig. 6). Furthermore, in the same periods, the concentration of some major chemical elements in the HA01 water showed anomalous changes (Skelton et al., 2019), possibly caused by the rupture of a hydrological barrier due to fluid overpressure and/or slow deformation.

4.8. Potential precursor interpretation

From the aforementioned results, we speculate that the following hydrogeochemical changes in trace element concentrations could contribute to the reliable forecasting of future geological events. In particular, we interpret that:

(1) the hydrogeochemical changes in B, Al, Mo and Li, V, Ga concentrations recorded before and immediately after the onset of the 2014 Bárðarbunga eruption are potential remote volcanic precursors and inceptive post-cursors of this event, respectively.

(2) the hydrogeochemical changes in Li, B, Ga, Mo, Sr, Rb and Fe concentrations that occurred before the 2018 M_w 5.2 earthquake are potential earthquake precursors, indicating that trace elements may be hydrogeochemically sensitive to pre-seismic crustal deformation, particularly for earthquakes of an intermediately strong magnitude.

Our interpretations have to be further confirmed and validated by future hydrogeochemical monitoring, which must always include the analyses of major elements and isotopes of groundwater to obtain a complete overview.

5. Conclusions

Long-term hydrogeochemical monitoring of trace elements is a promising method for identifying potential precursors to significant geological events, such as $M_w \geq 5$ earthquakes and remote volcanic eruptions. This method should be integrated by further hydrogeochemical monitoring, such as concentrations of major elements and isotopes in groundwater. The role of each element (major, trace and isotope) as a potential precursor can be different and should be clearly identified and understood as a function of many influencing factors, such as site-specificity (i.e. subsurface geology) and type, distance and magnitude of geological events (e.g. earthquakes or volcanic eruptions).

The obtained results confirm that B is highly mobile during water–rock interaction in a basaltic-hosted geothermal system. Therefore, this trace element shows a relevant volcanic hydro-sensitivity as it is a good indicator of rock leaching.

PCA can help identify the specific role of elements in different events, highlighting that approximately 115 events can be better explained by major constituents (e.g. 2012 and 2013 $M_w > 5$ earthquakes) and other trace elements (e.g. 2014 Bárðarbunga eruption; 2018 M_w 5.2 earthquake). CP detection of a specific cluster of elements identified by PCA helps to statistically validate the trend variability in the time series. The trace elements showed different behaviours between volcanic and tectonic earthquakes and between the $M_w > 5$ tectonic earthquakes occurring in 2012–2013 and 2018. In particular, the contributions of modern-day groundwater affected by water–rock interaction that occurred one year before the 2012 earthquake seem to be coeval with the CPs detected in the concentration trends of Al, Mo and Ga.

The combined use of PCA and CP helps to eliminate the human influence in evaluating chemical concentration changes in groundwater samples collected in a time series. In particular, in long-term borehole monitoring, such as for HA01, the data reduction capability of PCA was useful to understand what trace elements (components) and samples (loadings) deserved particular attention. After that, the time series analysis by CP detection on those specific trace elements was helpful to confirm whether the trends had significant changes during a seismic or volcanic event. Both statistical tools help to reduce background and other redundant data variability typical of trace elements monitoring.

Pre- and post-eruptive hydrogeochemical changes in the groundwater from the HA01 borehole, which is located farther than 140 km from the Bárðarbunga volcano, should not be surprising. All seismically active faults have envelopes of critically high-pressure pore fluids. Indeed, an increase in stress accumulation was detected at the HFF system before the Bárðarbunga volcanic seismic crisis (Hong et al., 2020). Consequently, although both stations monitoring shear-wave splitting and the HA01 borehole in northern Iceland are well over 100 km from Bárðarbunga, they seem to be sensitive to stress changes that when recording stress accumulation and chemical variations before the Bárðarbunga eruption.

Certainly, the diffusion of long-term hydrogeochemical monitoring sites and networks over seismic and volcanic territories will allow scientists to make significant progress in the science of geological risk precursors (Franchini et al., 2020).

Supplementary data to this article can be found online at https://doi.org/10.1016/j.scitotenv.2021.148635.

CRediT authorship contribution statement

Maurizio Barbieri: Conceptualization, Methodology, Data curation, Writing – review & editing. **Stefania Franchini:** Methodology, Formal analysis, Data curation, Writing – review & editing. **Marino Domenico Barberio:** Methodology, Formal analysis, Data curation, Writing – review & editing. **Andrea Billi:** Conceptualization, Methodology, Data curation, Writing – review & editing. **Tiziano Boschetti:** Conceptualization, Methodology, Data curation, Writing – review & editing. **Livio Giansante:** Formal analysis. **Francesca Gori:** Methodology, Formal analysis, Data curation, Writing – review & editing. **Sigurjón Jónsson:** Methodology, Data curation, Writing – review & editing. **Marco Petitta:** Conceptualization, Methodology, Data curation, Writing – review & editing. **Alasdair Skelton:** Conceptualization, Methodology, Data curation, Writing – review & editing. **Gabrielle Stockmann:** Methodology, Data curation, Writing – review & editing.

Declaration of competing interest

The authors declare that they have no known competing financial interests or personal relationships that could have appeared to influence the work reported in this paper.

Acknowledgements

This research was partly funded by Fondi di Ateneo, Sapienza University of Rome and partly by Fondazione ANIA (www.fondazioneania.it) through the HydroQuakes Project that involves Fondazione ANIA, Istituto di Geologia Ambientale e Geoingegneria (IGAG-CNR) and Sapienza University of Rome. We thank Dr Umberto Guidoni (Fondazione ANIA) and his collaborators for granting the permit to publish these results. We thank Hreinn Hjartarson for his help in collecting all of the groundwater samples. The authors thank the Associate Editor and three anonymous reviewers for their constructive comments.

References

Aiuppa, A., Allard, P., D'Alessandro, W., Michel, A., Parello, F., Treuil, M., Valenza, M., 2000. Mobility and fluxes of major, minor and trace metals during basalt weathering and groundwater transport at Mt. Etna volcano (Sicily). Geochim. Cosmochim. Acta 64, 1827–1841. https://doi.org/10.1016/S0016-7037(00)00345-8.

Aiuppa, A., Moretti, R., Federico, C., Giudice, G., Gurrieri, S., Liuzzo, M., Papale, P., Shinohara, H., Valenza, M., 2007. Forecasting Etna eruptions by real-time observation of volcanic gas composition. Geology 35, 1115–1118. https://doi.org/10.1130/G24149A.1.

Andrén, M., Stockmann, G., Skelton, A., Sturkell, E., Mörth, C.M., Guðrúnardóttir, H.R., Keller, N.S., Odling, N., Dahrén, B., Broman, C., Balic-Zunic, T., Hjartarson, H., Siegmund, H., Freund, F., 2016. Coupling between mineral reactions, chemical changes in groundwater, and earthquakes in Iceland. J. Geophys. Res. Solid Earth 121, 2315–2337. https://doi.org/10.1002/2015JB012614.

Armienta, M.A., De la Cruz-Reyna, S., 1995. Some hydro-geochemical fluctuations observed in Mexico related to volcanic activity. Appl. Geochem. 10 (2), 215–227. https://doi.org/10.1016/0883-2927(94)00044-7.

Armienta, M.A., De la Cruz-Reyna, S., Gómez, A., Ramos, E., Ceniceros, N., Cruz, O., Aguayo, A., Martínez, A., 2008. Hydrogeochemical indicators of the Popocatépetl volcano activity. J. Volcanol. Geotherm. Res. 170, 35–50. https://doi.org/10.1016/j.jvolgeores.2007.09.006.

Árnadottir, T., Geirsson, H., Jiang, W., 2008. Crustal deformation in Iceland: plate spreading and earthquake deformation. Jökull. 58, 59–74.

Árnason, K., 2020. New conceptual model for the magma-hydrothermal-tectonic system of Krafla, NE Iceland. Geosciences 10 (1), 34. https://doi.org/10.3390/geosciences10010034.

Arnórsson, S., 1969. A Geochemical Study of Selected Elements in Thermal Waters of Iceland. Ph.D. Thesis. Faculty of Science of the University of London, Royal School of Mines, Imperial College.

Arnórsson, S., Andrésdóttir, A., 1995. Processes controlling the distribution of boron and chlorine in natural waters in Iceland. Geochim. Cosmochim. Acta 59, 4125–4146. https://doi.org/10.1016/0016-7037(95)00278-8.

Arnórsson, S., Óskarsson, N., 2007. Molybdenum and tungsten in volcanic rocks and in surface and < 100 C ground waters in Iceland. Geochim. Cosmochim. Acta 71, 284–304. https://doi.org/10.1016/j.gca.2006.09.030.

Awaleh, M.O., Boschetti, T., Adaneh, A.E., Daoud, M.A., Ahmed, M.M., Dabar, O.A., Soubaneh, Y.D., Kawalieh, K.D., Kadieh, I.H., 2020. Hydrochemistry and multi-isotope study of the waters from Hanlé-Gaggadé grabens (Republic of Djibouti, East African Rift System): a low-enthalpy geothermal resource from a transboundary aquifer. Geothermics 86, 101805. https://doi.org/10.1016/j.geothermics.2020.101805.

Barberio, M.D., Barbieri, M., Billi, A., Doglioni, C., Petitta, M., 2017. Hydrogeochemical changes before and during the 2016 Amatrice-Norcia seismic sequence (central Italy). Sci. Rep. 7, 11735. https://doi.org/10.1038/s41598-017-11990-8.

Barberio, M.D., Gori, F., Barbieri, M., Billi, A., Caracausi, A., De Luca, G., Franchini, S., Petitta, M., Doglioni, C., 2020. New observations in Central Italy of groundwater responses to the worldwide seismicity. Sci. Rep. 10, 17850. https://doi.org/10.1038/s41598-020-74991-0.

Barbieri, M., 2019. Isotopes in hydrology and hydrogeology. Water (Switzerland) 11 (2), 291. https://doi.org/10.3390/w11020291.

Barbieri, M., Boschetti, T., Barberio, M.D., Billi, A., Franchini, S., Iacumin, P., Selmo, E., Petitta, M., 2020. Tracing deep fluid source contribution to groundwater in an active seismic area (central Italy): a combined geothermometric and isotopic (δ13C) perspective. J. Hydrol. 582, 124495. https://doi.org/10.1016/j.jhydrol.2019.124495.

Berger, G., Schott, J., Guy, C., 1988. Behavior of Li, Rb and Cs during basalt glass and olivine dissolution and chlorite, smectite and zeolite precipitation from seawater: experimental investigations and modelization between 50 and 300 C. Chem. Geol. 71, 297–312. https://doi.org/10.1016/0009-2541(88)90056-3.

Blomgren, V.J., Crossey, L.J., Karlstrom, K.E., Fischer, T.P., Darrah, T.H., 2019. Hot spring hydrochemistry of the Rio Grande rift in northern New Mexico reveals a distal geochemical connection between Valles Caldera and Ojo Caliente. J. Volcanol. Geotherm. Res. 387, 106663. https://doi.org/10.1016/j.jvolgeores.2019.106663.

Boschetti, T., Cortecci, G., Bolognesi, L., 2003. Chemical and isotopic compositions of the shallow groundwater system of Vulcano Island, Aeolian Archipelago, Italy: an update. GeoActa 2, 1–34.

Boschetti, T., Barbieri, M., Barberio, M.D., Billi, A., Franchini, S., Petitta, M., 2019. CO2 Inflow and elements desorption prior to a seismic sequence, Amatrice-Norcia 2016, Italy. Geochem. Geophys. Geosyst. 20 (5), 2303–2317. https://doi.org/10.1029/2018GC008117.

Bryant, F.D., Yarnold, P.R., 1995. Principal components analysis and exploratory and confirmatory factor analysis. In: Grimm, L.G., Yarnold, P.R. (Eds.), Reading and Understanding Multivariate Analysis. American Psychological Association Books.

Buttitta, D., Caracausi, A., Chiaraluce, L., Favara, R., Morticelli, M.G., Sulli, A., 2020. Continental degassing of helium in an active tectonic setting (northern Italy): the role of seismicity. Sci. Rep. 10, 1–13. https://doi.org/10.1038/s41598-019-55678-7.

Caracausi, A., Italiano, F., Paonita, A., Rizzo, A., Nuccio, P.M., 2003. Evidence of deep magma degassing and ascent by geochemistry of peripheral gas emissions at Mount Etna (Italy): assessment of the magmatic reservoir pressure. J. Geophys. Res. Solid Earth 108 (B10). https://doi.org/10.1029/2002JB002095.

Chaudhuri, H., Barman, C., Iyengar, A.S., Ghose, D., Sen, P., Sinha, B., 2013. Network of seismo-geochemical monitoring observatories for earthquake prediction research in India. Acta Geophys. 61, 1000–1025. https://doi.org/10.2478/s11600-013-0134-0.

Chen, C.H., Wang, C.H., Wen, S., Yeh, T.K., Lin, C.H., Liu, J.Y., Yen, H.Y., Lin, C., Rau, R.J., Lin, T.W., 2013. Anomalous frequency characteristics of groundwater level before major earthquakes in Taiwan. Hydrol. Earth Syst. Sci. 1, 1693. https://doi.org/10.5194/hess-17-1693-2013 2013.

Chen, C.H., Tang, C.C., Cheng, K.C., Wang, C.H., Wen, S., Lin, C.H., Wen, Y.Y., Meng, G., Yeh, T.K., Jan, J.C., Yen, H.Y., Liu, J.Y., 2015. Groundwater–strain coupling before the 1999 Mw 7.6 Taiwan Chi-Chi earthquake. J. Hydrol. 524, 378–384. https://doi.org/10.1016/j.jhydrol.2015.03.006.

Chiarabba, C., De Gori, P., Segou, M., Cattaneo, M., 2020. Seismic velocity precursors to the 2016 Mw 6.5 Norcia (Italy) earthquake. Geology. 48 (9), 924–928. https://doi.org/10.1130/G47048.1.

Chiodini, G., Cardellini, C., Di Luccio, F., Selva, J., Frondini, F., Caliro, S., Rosiello, A., Beddini, G., Ventura, G., 2020. Correlation between tectonic CO2 Earth degassing and seismicity is revealed by a 10-year record in the Apennines, Italy. Sci. Adv. 6. https://doi.org/10.1126/sciadv.abc2938 eabc2938.

Claesson, L., Skelton, A., Graham, C., Dietl, C., Mörth, M., Torssander, P., Kockum, I., 2004. Hydrogeochemical changes before and after a major earthquake. Geology 32, 641–644. https://doi.org/10.1130/G20542.1.

Claesson, L., Skelton, A., Graham, C., Mörth, C.M., 2007. The timescale and mechanisms of fault sealing and water-rock interaction after an earthquake. Geofluids 7 (4), 427–440. https://doi.org/10.1111/j.1468-8123.2007.00197.x.

Coppola, M., Correale, A., Barberio, M.D., Billi, A., Cavallo, A., Fondriest, M., Nazzari, M., Paonita, A., Romano, C., Stagno, V., Viti, C., Vona, A., 2021. Meso-to nano-scale evidence of fluid-assisted co-seismic slip along the normal Mt. Morrone Fault, Italy: implications for earthquake hydrogeochemical precursors. Earth Planet. Sci. Lett. https://doi.org/10.1016/j.epsl.2021.117010 in press.

Cucci, L., 2019. Insights into the geometry and faulting style of the causative faults of the M 6.7 1805 and M 6.7 1930 earthquakes in the Southern Apennines (Italy) from coseismic hydrological changes. Tectonophysics 751, 192–211. https://doi.org/10.1016/j.tecto.2018.12.021.

De Argollo, R.M., Schilling, J.G., 1978. Ge/Si and Ga/Al variations along the Reykjanes ridge and Iceland. Nature 276, 24–28. https://doi.org/10.1038/276024a0.

De Luca, G., Di Carlo, G., Tallini, M., 2018. A record of changes in the Gran Sasso groundwater before, during and after the 2016 Amatrice earthquake, central Italy. Sci. Rep. 8, 15982. https://doi.org/10.1038/s41598-018-34444-1.

De Moor, J.M., Aiuppa, A., Pacheco, J., Avard, G., Kern, C., Liuzzo, M., ... Fischer, T.P., 2016. Short-period volcanic gas precursors to phreatic eruptions: insights from Poás Volcano, Costa Rica. Earth Planet. Sci. Lett. 442, 218–227. https://doi.org/10.1016/j.epsl.2016.02.056.

Einarsson, P., 1991. Earthquakes and present-day tectonism in Iceland. Tectonophysics 189 (1-4), 261–279. https://doi.org/10.1016/0040-1951(91)90501-I.
Einarsson, P., Björnsson, S., 1979. Earthquakes in Iceland. Jökull 29, 37–43.
Einarsson, P., Theodórsson, P., Hjartardóttir, Á.R., Guðjónsson, G.I., 2008. Radon changes associated with the earthquake sequence in June 2000 in the South Iceland seismic zone. Terrestrial Fluids, Earthquakes and Volcanoes: The Hiroshi Wakita Volume III. Birkhäuser, Basel, pp. 63–74 https://doi.org/10.1007/978-3-7643-8738-9_5.
Elmi, S.A., 2009. Gallium and germanium distribution in geothermal water. Geothermal Training Programme, Reports. 2009, pp. 1–13.
Filzmoser, P., Todorov, V., 2013. Robust tools for the imperfect world. Inf. Sci. 245, 4–20. https://doi.org/10.1016/j.ins.2012.10.017.
Fournier, R.O., 1989. Lectures on Geochemical Interpretation of Hydrothermal Waters. UNU Geothermal Training Programme, Report 10. Reykjavik, Iceland, p. 73.
Fournier, R.O., Potter II, R.W., 1979. Magnesium correction to the Na-K-Ca chemical geothermometer. Geochim. Cosmochim. Acta 43, 1543–1550. https://doi.org/10.1016/0016-7037(79)90147-9.
Fournier, R.O., Truesdell, A.H., 1973. An empirical Na-K-Ca geothermometer for natural waters. Geochim. Cosmochim. Acta 37 (5), 1255–1275. https://doi.org/10.1016/0016-7037(73)90060-4.
Franchini, S., Agostini, S., Barberio, M.D., Barbieri, M., Billi, A., Boschetti, T., Pennisi, M., Petitta, M., 2020. HydroQuakes, central Apennines, Italy: towards a hydrogeochemical monitoring network for seismic precursors and the hydro-seismo-sensitivity of boron. J. Hydrol. 125754. https://doi.org/10.1016/j.jhydrol.2020.125754.
Gale, A., Dalton, C.A., Langmuir, C.H., Su, Y., Schilling, J.G., 2013. The mean composition of ocean ridge basalts. Geochem. Geophys. Geosyst. 14, 489–518. https://doi.org/10.1029/2012GC004334.
Galeczka, I., Eiriksdottir, E.S., Pálsson, F., Oelkers, E., Lutz, S., Benning, L.G., ... Ólafsdóttir, R., 2017. Pollution from the 2014–15 Bárðarbunga eruption monitored by snow cores from the Vatnajökull glacier, Iceland. J. Volcanol. Geotherm. Res. 347, 371–396. https://doi.org/10.1016/j.jvolgeores.2017.10.006.
Galeczka, I., Sigurdsson, G., Eiriksdottir, E.S., Oelkers, E.H., Gislason, S.R., 2016. The chemical composition of rivers and snow affected by the 2014/2015 Bárðarbunga eruption, Iceland. J. Volcanol. Geotherm. Res. 316, 101–119. https://doi.org/10.1016/j.jvolgeores.2016.02.017.
Garson, G.D., 2018. Factor Analysis. Statistical Associates, Blue Book Series 146 pp.
Giggenbach, W.F., 1991. Chemical techniques in geothermal exploration. In: D'Amore, F. (Ed.), Applications of Geochemistry in Geothermal Reservoir Development. UNITAR/UNDP publication, Rome, pp. 119–142.
Gislason, S.R., Arnorsson, S., Armannsson, H., 1996. Chemical weathering of basalt in Southwest Iceland; effects of runoff, age of rocks and vegetative/glacial cover. Am. J. Sci. 296, 837–907.
Gudmundsson, A., 2007. Infrastructure and evolution of ocean-ridge discontinuities in Iceland. J. Geodyn. 43, 6–29. https://doi.org/10.1016/j.jog.2006.09.002.
Gudmundsson, A., Brynjolfsson, S., Jonsson, M.T., 1993. Structural analysis of a transform fault-rift zone junction in North Iceland. Tectonophysics 220, 205–221. https://doi.org/10.1016/0040-1951(93)90232-9.
Gudmundsson, M.T., Jónsdóttir, K., Hooper, A., Holohan, E.P., Halldórsson, S.A., Ófeigsson, B.G., Cesca, S., Vogfjörd, K.S., Sigmundsson, F., Högnadóttir, T., Einarsson, P., Sigmarsson, O., Jarosch, A.H., Jónasson, K., Magnússon, E., Hreinsdóttir, S., Bagnardi, M., Parks, M.M., Hjörleifsdóttir, V., Pálsson, F., Walter, T.R., Schöpfer, M.P.J., Heimann, S., Reynolds, H.I., Dumont, S., Bali, E., Gudfinnsson, G.H., Dahm, T., Roberts, M.J., Hensch, M., Belart, J.M.C., Spaans, K., Jakobsson, S., Gudmundsson, G.B., Fridriksdóttir, H.M., Drouin, V., Dürig, T., Aðalgeirsdóttir, G., Riishuus, M.S., Pedersen, G.B.M., van Boeckel, T., Oddsson, B., Pfeffer, M.A., Barsotti, S., Bergsson, B., Donovan, A., Burton, M.R., Aiuppa, A., 2016. Gradual caldera collapse at Bárdarbunga volcano, Iceland, regulated by lateral magma outflow. Science 353. https://doi.org/10.1126/science.aaf8988.
Hatcher, L., O'Rourke, N., 2013. A Step-by-step Approach to Using the SAS® System for Factor Analysis and Structural Equation Modeling - Second Edition. SAS Institute Inc., Cary, North Carolina, USA.
He, A., Singh, R.P., 2019. Coseismic groundwater temperature response associated with the Wenchuan earthquake. Pure Appl. Geophys. 177 (1), 109–120. https://doi.org/10.1007/s00024-019-02097-4.
Hong, Q., Crampin, S., Gao, Y., 2020. Changes in shear-wave splitting at the 2014 Bárðarbunga seismic crisis and dyke intrusion in Iceland compared with earthquakes and other eruptions. Phys. Earth Planet. Inter. 300, 106446. https://doi.org/10.1016/j.pepi.2020.106446.
Hosono, T., Masaki, Y., 2020. Post-seismic hydrochemical changes in regional groundwater flow systems in response to the 2016 Mw 7.0 Kumamoto earthquake. J. Hydrol. 580, 124340. https://doi.org/10.1016/j.jhydrol.2019.124340.
Hosono, T., Yamada, C., Manga, M., Wang, C.Y., Tanimizu, M., 2020. Stable isotopes show that earthquakes enhance permeability and release water from mountains. Nat. Commun. 11, 1–9. https://doi.org/10.1038/s41467-020-16604-y.
Hubert, M., Reynkens, T., Schmitt, E., Verdonck, T., 2016. Sparse PCA for high-dimensional data with outliers. Technometrics 58 (4), 424–434. https://doi.org/10.1080/00401706.2015.1093962.
Hutcheson, G., Sofroniou, N., 1999. The Multivariate Social Scientist: Introductory Statistics Using Generalized Linear Models. Sage Publications, Thousand Oaks, CA.
IBM, 2019. IBM SPSS Statistics Base 26. Copyright IBM Corp. 1989. 2019. https://www.ibm.com/support/pages/ibm-spss-statistics-26-documentation.
Igarashi, G., Saeki, S., Takahata, N., Sumikawa, K., Tasaka, S., Sasaki, Y., Takahashi, M., Sano, Y., 1995. Ground-water radon anomaly before the Kobe earthquake in Japan. Science 269, 60–61. https://doi.org/10.1126/science.269.5220.60.
Ilgen, A.G., Kukkadapu, R.K., Leung, K., Washington, R.E., 2019. "Switching on" iron in clay minerals. Environ. Sci. Nano 6, 1704–1715. https://doi.org/10.1039/C9EN00228F.
IMO, 2016. Icelandic Meteological Office. www.vedur.is. (Accessed 22 December 2020).
Ingebritsen, S.E., Manga, M., 2014. Earthquakes: hydrogeochemical precursors. Nat. Geosci. 7, 697–698. https://doi.org/10.1038/ngeo2261.
Jóhannesson, H., 2014. Geological Map of Iceland 1:600 000. Bedrock Geology. 2nd edition. Icelandic Institute of Natural History, Reykjavik.
Joinpoint Regression Program, 2020. Version 4.8.0.1 - April 2020; Statistical Methodology and Applications Branch, Surveillance Research Program. National Cancer Institute https://surveillance.cancer.gov/joinpoint/Joinpoint_Help_4.8.0.1.pdf. (Accessed 22 December 2020).
Jónsson, S., Matrau, R., Viltres, R., Ófeigsson, B., 2019. An update of GPS measurements in north Iceland. In: Jónsson, S., et al. (Eds.), Proceedings to the Northquake 2019 Workshop. Húsavík Academic Centre , pp. 107–110. https://hac.is/wp-content/uploads/Northquake2019.pdf.
Jung, H.W., Yun, S.T., Kim, K.H., Oh, S.S., Kang, K.G., 2014. Role of an impermeable layer in controlling groundwater chemistry in a basaltic aquifer beneath an agricultural field, Jeju Island, South Korea. Appl. Geochem. 45, 82–93. https://doi.org/10.1016/j.apgeochem.2014.03.008.
Kaasalainen, H., Stefánsson, A., 2012. The chemistry of trace elements in surface geothermal waters and steam, Iceland. Chem. Geol. 330, 60–85. https://doi.org/10.1016/j.chemgeo.2012.08.019.
Kaasalainen, H., Stefánsson, A., Giroud, N., Arnórsson, S., 2015. The geochemistry of trace elements in geothermal fluids, Iceland. Appl. Geochem. 62, 207–223. https://doi.org/10.1016/j.apgeochem.2015.02.003.
Kawabata, K., Sato, T., Takahashi, H.A., Tsunomori, F., Hosono, T., Takahashi, M., Kitamura, Y., 2020. Changes in groundwater radon concentrations caused by the 2016 Kumamoto earthquake. J. Hydrol. 584, 124712. https://doi.org/10.1016/j.jhydrol.2020.124712.
Kim, H.J., Feuer, E.J., Midhune, D.N., 2000. Permutation tests for joinpoint regression with applications to cancer rates. Stat. Med. 19, 335–351. https://doi.org/10.1002/(SICI)1097-0258(20000215)19:3<335::AID-SIM336>3.0.CO;2-Z.
Kim, J., Kim, H.J., 2016. Consistent model selection in segmented line regression. J. Statist. Plann. Inference 170, 106–116.
Kim, J., Lee, J., Petitta, M., Kim, H., Kaown, D., Park, I.W., ... Lee, K.K., 2019. Groundwater system responses to the 2016 ML 5.8 Gyeongju earthquake, South Korea. J. Hydrol. 576, 150–163. https://doi.org/10.1016/j.jhydrol.2019.06.044.
King, C.Y., Zhang, W., Zhang, Z., 2006. Earthquake-induced groundwater and gas changes. Pure Appl. Geophys. 163, 633–645. https://doi.org/10.1007/s00024-006-0049-7.
Koh, D.C., Chae, G.T., Ryu, J.S., Lee, S.G., Ko, K.S., 2016. Occurrence and mobility of major and trace elements in groundwater from pristine volcanic aquifers in Jeju Island, Korea. Appl. Geochem. 65, 87–102. https://doi.org/10.1016/j.apgeochem.2015.11.004.
Kokfelt, T.F., Hoernle, K.A.J., Hauff, F., Fiebig, J., Werner, R., Garbe-Schönberg, D., 2006. Combined trace element and Pb-Nd–Sr-O isotope evidence for recycled oceanic crust (upper and lower) in the Iceland mantle plume. J. Petrol. 47, 1705–1749. https://doi.org/10.1093/petrology/egl025.
Kristmannsdóttir, H., 2008. Jarðhitaauðlindir: Tækifæri til atvinnusköpunar og byggðaeflingar á Norðausturlandi með heilsutengdri ferðaþjónustu. https://www.ferdamalastofa.is/static/files/upload/files/200892516292jardhitaaudlindir_hrefna.pdf.
Kristmannsdóttir, H., 2011. Grunnvatnsrannsóknir í Norðurþingi 2010. Report LV-2011/074, Landsvirkjun. http://gogn.lv.is/files/2011/2011-074.pdf.
Kristmannsdóttir, H., Klemensson, V., 2007. Grunnvatnsrannsóknir á Norðausturlandi - Skilgreining á grunnástandi og tillögur um framtíðareftirlit með hugsanlegum breytingum á grunnvatnsstraumum í kjölfar vinnslu á háhitasvæðum. Report LV-2007/086, Landsvirkjun. https://www.landsvirkjun.is/Media/Grunnvatnsrannsoknir_a_Nordausturlandi_2007.pdf.
Kristmannsdóttir, H., Guðrúnardóttir, H.R., Akureyri, H., 2009. Grunnvatnsrannsóknir í Norðurþingi 2008. Report LV-2009/147, Landsvirkjun. https://www.landsvirkjun.is/Media/Grunnvatnsrannsoknir_i_Nordurthingi_2008.pdf.
Kristmannsdóttir, H., Arnórsson, S., Sveinbjörnsdóttir, A.E., Ármannsson, H., 2010. Chemical variety of water in Icelandic heating systems. Proceedings of the World Geothermal Congress 2010. 1477, pp. 1–9.
Li, S., Sigmundsson, F., Drouin, V., Parks, M.M., Ofeigsson, B.G., Jónsdóttir, K., ... Hreinsdóttir, S., 2021. Ground deformation after a caldera collapse: contributions of magma inflow and viscoelastic response to the 2015–2018 deformation field around Bárðarbunga, Iceland. J. Geophys. Res. Solid Earth 126 (3). https://doi.org/10.1029/2020JB020157.
Ma, L., Qian, J., Zhao, W., Curtis, Z., Zhang, R., 2016. Hydrogeochemical analysis of multiple aquifers in a coal mine based on nonlinear PCA and GIS. Environ. Earth Sci. 75, 716. https://doi.org/10.1007/s12665-016-5532-6.
Manga, M., Wang, C.Y., 2015. 4.12. Earthquake hydrology. Treatise on Geophysics. 328, p. 305. https://doi.org/10.1016/B978-0-444-53802-4.00082-8.
Manga, M., Brodsky, E.E., Boone, M., 2003. Response of streamflow to multiple earthquakes. Geophys. Res. Lett. 30 (5). https://doi.org/10.1029/2002GL016618.
Marcovecchio, J.E., Botté, S.E., Domini, C.E., Freije, R.H., 2014. Heavy metals, major metals, trace elements. In: Nollet, L.M.L., De Gelder, L.S.P. (Eds.), Handbook of Water Analysis, Chapter 15. Taylor & Francis Group, Boca Raton, Florida, pp. 385–434 https://doi.org/10.1201/b15314-19.
Marini, L., 2013. Reaction path modeling: theoretical aspects and applications. In: Censi, P., Darrah, T.H., Yigal, Erel Y. (Eds.), Medical Geochemistry - Geological Materials and Health, Chapter 4. Springer, Dordrecht, pp. 47–66 https://doi.org/10.1007/978-94-007-4372-4_4.
Martinelli, G., Facca, G., Genzano, N., Gherardi, F., Lisi, M., Pierotti, L., Tramutoli, V., 2020. Earthquake-related signals in central Italy detected by hydrogeochemical and satellite techniques. Front. Earth Sci. 8, 584716. https://doi.org/10.3389/feart.2020.584716.

Marzocchi, W., Bebbington, M.S., 2012. Probabilistic eruption forecasting at short and long time scales. Bull. Volcanol. 74, 1777–1805. https://doi.org/10.1007/s00445-012-0633-x.
McNutt, S.R., Roman, D.C., 2015. Volcanic seismicity. The Encyclopedia of Volcanoes. Academic Press, pp. 1011–1034 https://doi.org/10.1016/B978-0-12-385938-9.00059-6.
Montgomery, D.R., Manga, M., 2003. Streamflow and water well responses to earthquakes. Science 300, 2047–2049. https://doi.org/10.1126/science.1082980.
Nakagawa, K., Yu, Z.Q., Berndtsson, R., Hosono, T., 2020. Temporal characteristics of groundwater chemistry affected by the 2016 Kumamoto earthquake using self-organizing maps. J. Hydrol. 582, 124519. https://doi.org/10.1016/j.jhydrol.2019.124519.
Nicholson, K., 1993. Geothermal Fluids: Chemistry and Exploration Techniques. Springer Science & Business Media.
Nigro, A., Sappa, G., Barbieri, M., 2017. Application of boron and tritium isotopes for tracing landfill contamination in groundwater. J. Geochem. Explor. 172, 101–108. https://doi.org/10.1016/j.gexplo.2016.10.011.
Oelkers, E.H., Bénézeth, P., Pokrovski, G.S., 2009. Thermodynamic databases for water-rock interaction. Rev. Mineral. Geochem. 70, 1–46. https://doi.org/10.2138/rmg.2009.70.1.
Onda, S., Sano, Y., Takahata, N., Kagoshima, T., Miyajima, T., Shibata, T., Pinti, D.L., Lan, T., Kim, N.K., Kusakabe, M., Nishio, Y., 2018. Groundwater oxygen isotope anomaly before the M6. 6 Tottori earthquake in Southwest Japan. Sci. Rep., 1–7 https://doi.org/10.1038/s41598-018-23303-8.
OriginLab, 2019. Principal Component Analysis. Origin Help, Section 17.7.1. https://www.originlab.com/doc/Origin-Help/PrincipleComp-Analysis. (Accessed 20 July 2020).
Patanè, D., De Gori, P., Chiarabba, C., Bonaccorso, A., 2003. Magma ascent and the pressurization of Mount Etna's volcanic system. Science 299, 2061–2063. https://doi.org/10.1126/science.1080653.
Petitta, M., Mastrorillo, L., Preziosi, E., Banzato, F., Barberio, M.D., Billi, A., Cambi, C., De Luca, G., Di Carlo, G., Di Curzio, D., Di Salvo, C., Nanni, T., Palpacelli, S., Rusi, S., Saroli, M., Tallini, M., Tazioli, A., Valigi, D., Vivalda, P., Doglioni, C., 2018. Water-table and discharge changes associated with the 2016–2017 seismic sequence in central Italy: hydrogeological data and a conceptual model for fractured carbonate aquifers. Hydrogeol. J. 26, 1009–1026. https://doi.org/10.1007/s10040-017-1717-7.
Reimann, C., De Caritat, P., 1998. Chemical Elements in the Environment: Factsheets for the Geochemist and Environmental Scientist. Springer Science & Business Media.
Reynolds, H.I., Gudmundsson, M.T., Högnadóttir, T., Axelsson, G., 2019. Changes in geothermal activity at Bárdarbunga, Iceland, following the 2014–2015 caldera collapse, investigated using geothermal system modeling. J. Geophys. Res. Solid Earth 124, 8187–8204. https://doi.org/10.1029/2018JB017290.
Ricolfi, L., Barbieri, M., Muteto, P.V., Nigro, A., Sappa, G., Vitale, S., 2020. Potential toxic elements in groundwater and their health risk assessment in drinking water of Limpopo National Park, Gaza Province, Southern Mozambique. Environ. Geochem. Health, 1–13 https://doi.org/10.1007/s10653-019-00507-z.
Rögnvaldsson, S.T., Gudmundsson, A., Slunga, R., 1998. Seismotectonic analysis of the Tjörnes Fracture Zone, an active transform fault in north Iceland. J. Geophys. Res. Solid Earth 103, 30117–30129. https://doi.org/10.1029/98JB02789.
Ruch, J., Wang, T., Xu, W., Hench, M., Jónsson, S., 2016. Oblique rift opening revealed by recurring magma injection in central Iceland. Nat. Commun. 7, 12352. https://doi.org/10.1038/ncomms12352.
Sano, Y., Takahata, N., Kagoshima, T., Shibata, T., Onoue, T., Zhao, D., 2016. Groundwater helium anomaly reflects strain change during the 2016 Kumamoto earthquake in Southwest Japan. Sci. Rep. 6, 37939. https://doi.org/10.1038/srep37939.
Sano, Y., Onda, S., Kagoshima, T., Miyajima, T., Takahata, N., Shibata, T., Nakagawa, C., Onoue, T., Kim, N.K., Lee, H., Kusakabe, M., Pinti, D.L., 2020. Groundwater oxygen anomaly related to the 2016 Kumamoto earthquake in Southwest Japan. Proc. Jpn. Acad. Ser. B 96, 322–334. https://doi.org/10.2183/pjab.96.024.
Sato, T., Takahashi, H.A., Kawabata, K., Takahashi, M., Inamura, A., Handa, H., 2020. Changes in the nitrate concentration of spring water after the 2016 Kumamoto earthquake. J. Hydrol. 580, 124310. https://doi.org/10.1016/j.jhydrol.2019.124310.
Schoeller, H., 1962. Les Eaux souterraines: hydrologie, dynamique et chimique, recherche, exploitation et évaluation des ressources. 642. Masson et Cie, Paris.
Scholz, C.H., Sykes, L.R., Aggarwal, Y.P., 1973. Earthquake prediction: a physical basis. Science 181, 803–810.
Seyfried Jr., W.E., Bischoff, J.L., 1979. Low temperature basalt alteration by sea water: an experimental study at 70 C and 150 C. Geochim. Cosmochim. Acta 43, 1937–1947. https://doi.org/10.1016/0016-7037(79)90006-1.
Seyfried Jr., W.E., 1987. Experimental and theoretical constraints on hydrothermal alteration processes at mid-ocean ridges. Annu. Rev. Earth Planet. Sci. 15, 317–335. https://doi.org/10.1146/annurev.ea.15.050187.001533.
Shi, Z., Wang, G., 2014. Hydrological response to multiple large distant earthquakes in the Mile well, China. J. Geophys. Res. Earth Surf. 119, 2448–2459. https://doi.org/10.1002/2014JF003184.
Shi, Z., Zhang, H., Wang, G., 2020. Groundwater trace elements change induced by M5. 0 earthquake in Yunnan. J. Hydrol. 581, 124424. https://doi.org/10.1016/j.jhydrol.2019.124424.
Shorttle, O., Maclennan, J., Piotrowski, A.M., 2013. Geochemical provincialism in the Iceland plume. Geochim. Cosmochim. Acta 122, 363–397. https://doi.org/10.1016/j.gca.2013.08.032.
Sigmundsson, F., Hooper, A., Hreinsdóttir, S., Vogfjörd, K.S., Ófeigsson, B.G., Heimisson, E.R., Dumont, S., Parks, M., Spaans, K., Gudmundsson, G.B., Drouin, V., Árnadóttir, T., Jónsdóttir, K., Gudmundsson, M.T., Högnadóttir, T., Fridriksdóttir, H.M., Hensch, M., Einarsson, P., Magnússon, E., Samsonov, S., Brandsdóttir, B., White, R.S., Ágústsdóttir, T., Greenfield, T., Green, R.G., Hjartardóttir, Á.R., Pedersen, R., Bennett, R.A., Geirsson, H., La Femina, P.C., Björnsson, H., Pálsson, F., Sturkell, E., Bean, C.J., Möllhoff, M., Braiden, A.K., Eibl, E.P.S., 2015. Segmented lateral dyke growth in a rifting event at Bárðarbunga volcanic system, Iceland. Nature 517, 191–195. https://doi.org/10.1038/nature14111.
Skalska, H., 2017. Software for Changepoints Detection. Mathematical Methods in Economics 2017, Conference Proceedings, September 13th - 15th, 2017. University of Hradec Králové, Czech Republic.
Skelton, A., Andrén, M., Kristmannsdóttir, H., Stockmann, G., Mörth, C.M., Sveinbjörnsdóttir, Á., Jónsson, S., Sturkell, E., Guðrúnardóttir, H.R., Hjartarson, H., Siegmund, H., Kockum, I., 2014. Changes in groundwater chemistry before two consecutive earthquakes in Iceland. Nat. Geosci. 7, 752. https://doi.org/10.1038/ngeo2250.
Skelton, A., Claesson, L., Wästeby, N., Andrén, M., Stockmann, G., Sturkell, E., Mörth, C.M., Stefansson, A., Tollefsen, E., Siegmund, H., Keller, N., Kjartansdóttir, R., Hjartarson, H., Kockum, I., 2019. Hydrochemical changes before and after earthquakes based on long-term measurements of multiple parameters at two sites in Northern Iceland—a review. J. Geophys. Res. Solid Earth 124, 2702–2720. https://doi.org/10.1029/2018JB016757.
Sparks, R.S.J., 2003. Forecasting volcanic eruptions. Earth Planet. Sci. Lett. 210, 1–15. https://doi.org/10.1016/S0012-821X(03)00124-9.
Stefansson, R., Gudmundsson, G.B., Halldorsson, P., 2008. Tjörnes fracture zone. New and old seismic evidences for the link between the North Iceland rift zone and the Mid-Atlantic ridge. Tectonophysics 44, 117–126. https://doi.org/10.1016/j.tecto.2006.09.019.
Thordarson, T., Larsen, G., 2007. Volcanism in Iceland in historical time: volcano types, eruption styles and eruptive history. J. Geodyn. 43, 118–152. https://doi.org/10.1016/j.jog.2006.09.005.
Tibaldi, A., Corti, N., Bonali, F.L., Mariotto, F.P., Russo, E., 2020. Along-rift propagation of Pleistocene-Holocene faults from a central volcano. J. Struct. Geol. 141, 104201. https://doi.org/10.1016/j.jsg.2020.104201.
Trick, J.K., Stuart, M., Reeder, S., 2008. Contaminated groundwater sampling and quality control of water analyses. Environmental Geochemistry. Chapter 3 - Environmental Geochemistry (Second Edition). Site Characterization, Data Analysis and Case Histories. . Elsevier, pp. 29–45 https://doi.org/10.1016/B978-0-4.
Van Vliet-Lanoë, B., Bergerat, F., Allemand, P., Innocentd, C., Guillou, H., Cavailhes, T., Guðmundsson, Á., Chazot, G., Schneider, J.L., Grandjean, P., Liorzou, C., Passot, S., 2020. Tectonism and volcanism enhanced by deglaciation events in southern Iceland. Quat. Res. 94, 94–120. https://doi.org/10.1017/qua.2019.68.
Verma, M.P., Santoyo, E., 1997. New improved equations for Na/K, Na/Li and SiO2 geothermometers by outlier detection and rejection. J. Volcanol. Geotherm. Res. 79, 9–24. https://doi.org/10.1016/S0377-0273(97)00024-3.
Vigier, N., Burton, K.W., Gislason, S.R., Rogers, N.W., Duchene, S., Thomas, L., Hodge, E., Schaefer, B., 2006. The relationship between riverine U-series disequilibria and erosion rates in a basaltic terrain. Earth Planet. Sci. Lett. 249, 258–273. https://doi.org/10.1016/j.epsl.2006.07.001.
Wakita, H., 1975. Water wells as possible indicators of tectonic strain. Science 189, 553–555. https://doi.org/10.1126/science.189.4202.553.
Wakita, H., Nakamura, Y., Notsu, K., Noguchi, M., Asada, T., 1980. Radon anomaly: a possible precursor of the 1978 Izu-Oshima-kinkai earthquake. Science 207, 882–883. https://doi.org/10.1126/science.207.4433.882.
Wang, C.-Y., Manga, M., 2021. Water and Earthquakes. Springer Nature Switzerland AG, Cham, Switzerland https://doi.org/10.1007/978-3-030-64308-9.
Wästeby, N., Skelton, A., Tollefsen, E., Andrén, M., Stockmann, G., Claesson, L., Sturkell, E., Mörth, M., 2014. Hydrochemical monitoring, petrological observation, and geochemical modeling of fault healing after an earthquake. J. Geophys. Res. Solid Earth 119, 5727–5740. https://doi.org/10.1002/2013JB010715.
Willis, J.P., 1979. Some aspects of the geochemistry of gallium in silicate rocks and stoney meteorites. Ph.D. Thesis, 2nd ed University of Cape Town, unpublished.
Zhou, Z., Wang, J., Su, R., Guo, Y., Zhao, J., Zhang, M., Ji, R., Li, Y., Li, J., 2020. Hydrogeochemical and isotopic characteristics of groundwater in Xinchang preselected site and their implications. Environ. Sci. Pollut. Res. 27, 34734–34745. https://doi.org/10.1007/s11356-019-07208-1.